UNIVERSIDAD DE INVESTIGACIÓN DE TECNOLOGÍA EXPERIMENTAL YACHAY

Escuela de Ciencias Químicas e Ingeniería

TÍTULO: Study of High-Valent Iron Intermediates in Biological and Biomimetic Systems

Trabajo de integración curricular presentado como requisito para la obtención del título de Química

Autor:

Cordova Torres Airina Valentina

Tutor:

PhD. Saucedo Vázquez Juan Pablo

Urcuquí, agosto 2019

Urcuquí, 28 de agosto de 2019

SECRETARÍA GENERAL
(Vicerrectorado Académico/Cancillería)
ESCUELA DE CIENCIAS QUÍMICAS E INGENIERÍA
CARRERA DE QUÍMICA
ACTA DE DEFENSA No. UITEY-CHE-2019-00008-AD

En la ciudad de San Miguel de Urcuquí, Provincia de Imbabura, a los 28 días del mes de agosto de 2019, a las 09:30 horas, en el Aula AI-101 de la Universidad de Investigación de Tecnología Experimental Yachay y ante el Tribunal Calificador, integrado por los docentes:

Presidente Tribunal de Defensa	Dr. CAETANO , MANUEL SOUSA , Ph.D.
Miembro No Tutor	Dra. HIDALGO BONILLA, SANDRA PATRICIA , Ph.D.
Tutor	Dr. SAUCEDO VAZQUEZ, JUAN PABLO , Ph.D.

Se presenta el(la) señor(ita) estudiante **CORDOVA TORRES, AIRINA VALENTINA**, con cédula de identidad No. **1716844806**, de la **ESCUELA DE CIENCIAS QUÍMICAS E INGENIERÍA**, de la Carrera de **QUÍMICA**, aprobada por el Consejo de Educación Superior (CES), mediante Resolución **RPC-SO-39-No.456-2014**, con el objeto de rendir la sustentación de su trabajo de titulación denominado: **STUDY OF HIGH-VALENT IRON NTERMEDIATES IN BIOLOGICAL AND BIOMIMETIC SYSTEMS**, previa a la obtención del título de **QUÍMICO/A**.

El citado trabajo de titulación, fue debidamente aprobado por el(los) docente(s):

Tutor	Dr. SAUCEDO VAZQUEZ, JUAN PABLO , Ph.D.

Y recibió las observaciones de los otros miembros del Tribunal Calificador, las mismas que han sido incorporadas por el(la) estudiante.

Previamente cumplidos los requisitos legales y reglamentarios, el trabajo de titulación fue sustentado por el(la) estudiante y examinado por los miembros del Tribunal Calificador. Escuchada la sustentación del trabajo de titulación, que integró la exposición de el(la) estudiante sobre el contenido de la misma y las preguntas formuladas por los miembros del Tribunal, se califica la sustentación del trabajo de titulación con las siguientes calificaciones:

Tipo	Docente	Calificación
Presidente Tribunal De Defensa	Dr. CAETANO , MANUEL SOUSA , Ph.D.	10,0
Tutor	Dr. SAUCEDO VAZQUEZ, JUAN PABLO , Ph.D.	10,0
Miembro Tribunal De Defensa	Dra. HIDALGO BONILLA, SANDRA PATRICIA , Ph.D.	10,0

Lo que da un promedio de: **10 (Diez punto Cero)**, sobre 10 (diez), equivalente a: **APROBADO**

Para constancia de lo actuado, firman los miembros del Tribunal Calificador, el/la estudiante y el/la secretario ad-hoc.

CORDOVA TORRES, AIRINA VALENTINA
Estudiante

Dr. CAETANO , MANUEL SOUSA , Ph.D.
Presidente Tribunal de Defensa

Dr. SAUCEDO VAZQUEZ, JUAN PABLO , Ph.D.
Tutor

UNIVERSIDAD YACHAY TECH

Sandra P Hidalgo B

Dra. HIDALGO BONILLA, SANDRA PATRICIA , Ph.D.
Miembro No Tutor

ESCOBAR LANPAZURI, ANA MARIA
Secretario Ad-hoc

AUTORÍA

Yo, **AIRINA VALENTINA CORDOVA TORRES**, con cédula de identidad 1716844806, declaro que las ideas, juicios, valoraciones, interpretaciones, consultas bibliográficas, definiciones y conceptualizaciones expuestas en el presente trabajo; así cómo, los procedimientos y herramientas utilizadas en la investigación, son de absoluta responsabilidad de el/la autora (a) del trabajo de integración curricular. Así mismo, me acojo a los reglamentos internos de la Universidad de Investigación de Tecnología Experimental Yachay.

Urcuquí, agosto 2019.

Airina V Cordova T

Airina Valentina Cordova Torres
CI:1716844806

AUTORIZACIÓN DE PUBLICACIÓN

Yo, **AIRINA VALENTINA CORDOVA TORRES,** con cédula de identidad 1716844806, cedo a la Universidad de Tecnología Experimental Yachay, los derechos de publicación de la presente obra, sin que deba haber un reconocimiento económico por este concepto. Declaro además que el texto del presente trabajo de titulación no podrá ser cedido a ninguna empresa editorial para su publicación u otros fines, sin contar previamente con la autorización escrita de la Universidad.

Así mismo, autorizo a la Universidad que realice la digitalización y publicación de este trabajo de integración curricular en el repositorio virtual, de conformidad a lo dispuesto en el Art. 144 de la Ley Orgánica de Educación Superior

Urcuquí, agosto 2019.

Airina V Cordova T

Airina Valentina Cordova Torres
CI:1716844806

Dedicatoria

A mis dos madres, Mónica Torres por ser el bastión de mi vida que no permite que me rinda ante ninguna adversidad y a mi Katita Cruz por su entereza y solidaridad infinita.

A mi hermana, Eve Rojas y mi hermano Johancito Rojas para que se inspiren en las líneas del conocimiento científico y sean mejores seres humanos y profesionales.

Airina Valentina Cordova Torres

Agradecimiento

A Juan Pablo Saucedo, por permitirme trabajar con él codo a codo en esta laboriosa investigación y su apoyo como padre académico en el transcurso de mi carrera como Química.

A PhD. Wilhelm Hansberg Torres y su equipo de investigación en el Instituto de Fisiología Celular en la UNAM, por su apoyo incondicional en el desarrollo el presente trabajo.

A PhD. Marta Sosa por la orientación y apoyo así como también a Daniel Páez por sus incansables jornadas de laboratorio en la Facultad de Química, UNAM.

A Horte Rodríguez por ser una excelente madre académica. Marta López y Kamil por sus consejos.

A Keila Gómez, por su paciencia estos cinco años.

A la Escuela de Ciencias Químicas e Ingeniería y Departamento de Vicecancillería de la Universidad Experimental Yachay Tech, así como también al Instituto de Fundamento y Talento Humano IFTH por el apoyo financiero para desarrollar y culminar mis actividades de investigación en México y Ecuador condesadas en el presente trabajo

Airina Valentina Cordova Torres

PALABRAS PARA ELLA

"…Lo único estable es la felicidad, que no se compra ni se da en caridad…"

(P. Milanés)

Hablar de Valentina, es hablar de la década de los 90as, es rememorar aquel día que pidió venir a raudales de llanto en el que ya se reflejaba su rebeldía y su ganas de alumbrar con luz propia todo ese momento de estudio y de redescubrimiento. *Mientras que los hechos hubo que forzar, todo este triste mundo tendió a fracasar…,* un mundo de transformación que buscábamos con ahínco soñadores como su padre y yo, en una coyuntura en la que proyectar hijos para el cambio se hacía imprescindible e inevitable, *en la esperanza del que iba a nacer mis frustraciones todas las volqué…* Ella, hoy proyectada en la mujer que muchos conocen, llega a mi vida en el momento exacto que debía llegar, *era el perfecto aburrido fragor, de una búsqueda al centro del sol, quemando mi muerte, era la alegría de un pájaro gris con su canto pidiendo morir, porque estaba preso…*

Hablar de Valentina es hablar de proyectos e ilusiones posibles, reconocer por ejemplo que siempre ha luchado por lo que quiere: dotada de una fortaleza que alcanza límites inimaginables, tocar el corazón de muchos y aceptar el de pocos. "*Recuerdo el día exacto en el que te conocí, iba pegado al cielo y apenas te sentí, me descubriste todo/a de una vez y hacia tu mano abierta me lancé, en toda una persona hube de cambiar, gente respetable para acometer, todo un horario fijo para andar, un diario y la mesa, lista: a envejecer*... Si, ella vino rompiendo barreras, acabando con paradigmas, despojando prejuicios, aprendiendo que en la vida se llega con compañía, no obstante lanzarnos al vacío para conseguir metas propias y originales, en un acompañamiento sí, pero al que se depende de sí mismo, porque comprendió que en la consecución de las metas propias se hace necesario despojarse de pasiones y definitivamente enamorarse del camino de vida que se ve allá en lo alto de la expectativas de otros.

Hoy estoy aquí reconociendo los alcances de ella, mi Valen, reconociendo que nunca ha desistido: que rendirse en ella significa fracasar en los mil y uno intentos, porque siempre ha sido una mujer de decisión, dotada de persistencia que la ha llevado a donde hoy está. A pesar de la distancia la vida siempre la ha llevado a encontrarse en el camino a casa, a nuestros largos análisis de canciones y de búsquedas. La frustración no la hizo muñeca de papel, la fortaleza es su sino -como así lo entendiste desde niña- siempre encontraste motivos para derrumbar mis esquemas, encontrar alternativas viables a riesgo de transitar un camino desconocido pero siempre concertado (Gracias por apoyarte en mi). Las pequeñas cosas y los tropezones te enseñaron a crecer, porque al fin de cuentas la vida es eso: un aprender, un mejorar y un volver a intentarlo, pero sobre todo un engrandecer ese ser único y original que te representa desde aquel día en que te dije: mi niña tiene una estrella que le alumbrará por siempre su camino, *ahora junto al cielo me voy a quedar*, *quien me tienda la mano al pasar comparte mi suerte…*

Celebro tus logros, tu trabajo y tu esfuerzo: gracias por derribar esas barreras de la adversidad, gracias por romper con esas fronteras imaginarias, gracias por tu coraje, por alcanzar tus sueños, por tu paciencia y por tu soledad…Pero aquí estás y aquí estamos celebrando un peldaño más en la escala de tu vida, un encuentro con el mundo de las posibilidades, como nos enseñó la literatura, donde la mentira y la verdad convergen para amalgamarse en la grandeza de conocer, de creer en que sí se puede, si se visualiza desde nuestras propias ilusiones… Que seguir y avanzar en la ciencia, sea tu mayor y más sublime objetivo.

Te ama,

Tu madre.

PDN: Todas las citas en cursiva pertenecen al canta-autor cubano Pablo Milanés de su Poema canción: *Quien me tienda la mano al pasar. 1985.*

List of abbreviations

EPR: Electron Paramagnetic Resonance

LS: Low spin

HS: High spin

ROS: Reactive oxygen species

HOMO: Highest occupied molecular orbital

LUMO: Lowest Unoccupied Molecular Orbital

OS: Oxidation state

TNT: 2,4,6-Trinitrotoluene

CFT: Crystal field theory

LFT: Ligand field theory

IS: Inner sphere

OP: Outer sphere

NRVS: Nuclear resonance vibrational spectroscopy

N.crassa: Neurospora crassa fungus

CAT2: Catalase-peroxidase from *N.crassa*

Rz: Reinheitszahl ratio

PAA: Peroxyacetic acid.

MOT: Molecular Orbital Theory.

MO: Molecular Orbital

pheo: Pheophytin

Abstract

Ferryl intermediate compounds are relevant in catalytic mechanisms of dioxygen activation for a wide range of metalloproteins and inorganic synthetic compounds. In dioxygen activation, two mechanisms (inner and outer sphere) for the electronic transfer from iron to oxygen are recognized, from these, outer sphere mechanisms is most studied due to their importance in critical biological process. The presence of oxo-iron compounds with the central atom in high oxidation states (ferryl-Fe^{IV} and ferroyl-Fe^{V}) as reaction intermediates, makes this reactivity an exciting challenge for a chemist due to the difficulty for isolation and characterization of those species. Parallel to the research on biological systems, an important branch of Inorganic Chemistry has been developed in which the synthesis of inorganic compounds with structural characteristics and whose reactivity mimics the active sites of the metalloproteins helps to understand the biological processes.

In this work, the results of the isolation and characterization of a ferryl intermediate generated in the catalytic cycle of the bifunctional catalase-peroxidase (CAT2) enzyme of the *Neurospora crassa* fungus are presented. In particular, we worked with a variant of the CAT2 enzyme in which an amino acid (aspartate 120) critical for the catalase activity of the enzyme was mutated. The spectroscopic characterization by UV-Vis and EPR shows that the active site of the protein preserves iron with the same electronic structure as the native enzyme (HS-Fe^{III}), however, zymography displayed that catalase activity was severely affected while the peroxidase activity may still to be intact. Through a reaction with peroxyacetic acid (PAA) it was possible to artificially generate a ferryl intermediate which was characterized by UV-Vis and EPR spectroscopies, demonstrating the presence of Fe^{IV} and a free radical in a compound that is assigned to the species known as Compound I (Fe^{IV}=O $Por^{+}\bullet$).

On the other hand, in an effort to try to better understand the reaction mechanism of this bifunctional enzyme and others in which the reaction mechanism involves ferryl intermediates, in the second part of the work the results of the synthesis and characterization of a biomimetic compound are presented. One of the most important contributions of this part, is the proposal to use chlorophyll as a natural source for obtaining the porphyrin ligand for our compound, thus, the extraction of the spinach chlorophyll was made and magnesium was extracted to generate pheophytin ligand. The entire extraction process was carried out using chromatographic techniques, demonstrating the chemical composition of the extracts

in each step by electronic spectroscopy. A pheophytin-iron(II) complex was synthetized and characterized by UV-Vis and EPR spectroscopies, demonstrating the presence of the porphyrin ring of pheophytin and iron(II) LS. The evaluation of the reactivity of the compound against PAA was made by a preliminary kinetic study and EPR, demonstrating that PAA effectively reacts against iron, causing oxidation of the latter from Fe^{II} to Fe^{III}. Unfortunately, it was not possible to isolate a ferryl intermediate in this inorganic system, however, the fact of having demonstrated that the compound is capable of reacting against PAA is the basis for the construction of a biomimetic system in the very near future.

Key words
Oxo-iron; Biomimetic; catalase-peroxidase; Compound I; pheophytin; EPR;UV-VIs

Resumen

Los compuestos intermediarios ferrilos son relevantes en los mecanismos catalíticos durante la activación de oxígeno molecular en una amplia gama de metaloproteínas y compuestos sintéticos inorgánicos. En ese sentido, la activación de oxigeno ocurre a través de dos mecanismos de transferencia electrónica del átomo de hierro al oxígeno: esfera interna y esfera externa; es importante recalcar que el mecanismo de esfera externa es el más común en procesos de sistemas biológicos. La presencia de compuestos de hierro-oxígeno en los cuales el metal de transición se encuentra en altos estados de oxidación como intermediarios de reacción (ferril-Fe^{IV} y ferrol-Fe^{V}) hacen que esta reactividad sea un gran reto para un químico, debido a la dificultad que tiene el aislamiento y caracterización de dichas especies. Paralelo a esta investigación sobre sistemas biológicos, una importante rama de la química inorgánica se ha desarrollado, en esta, la síntesis de compuestos inorgánicos con características estructurales similares a los sitios activos de las metaloproteínas son capaces de imitar la reactividad de estas últimas, ayudando a comprender mucho mejor los procesos biológicos.

En el presente trabajo se presentan los resultados del aislamiento y caracterización de un intermediario ferrilo generado durante el ciclo catalítico de la enzima bi-funcional catalasa-peroxidasa (CAT2) obtenida a partir del hongo *Neurospora crassa*. Cabe señalar que nosotros trabajamos con una mutante de la CAT2 en la cual el aminoácido aspartato 120 que es crítico para la actividad de catalasa, fue modificado genéticamente. La caracterización espectroscópica fue llevada a cabo usando UV-Vis y RPE, los resultados muestran que el sitio activo de la proteína preserva el átomo de hierro con la misma estructura electrónica cuando es comparada con la enzima en su forma nativa (HS-Fe^{III}), sin embargo la zimografía demostró que la actividad de catalasa se ve afectada severamente mientras que la de peroxidasa está aún intacta. A través de una reacción con ácido peroxiacético fue posible generar un intermediario ferrilo de manera artificial el cual fue caracterizado mediante espectroscopias UV-Vis y RPE demostrando la presencia de Fe^{IV} y un radical libre en un compuesto que es asignado a especies conocidas como Compuesto I (Fe^{IV}=O $Por^{+}\bullet$).

Por otro lado en un esfuerzo de intentar entender el mecanismo de reacción de esta enzima bi-funcional y otras en las cuales el mecanismo de reacción envuelve la formación

de intermediarios ferrilos, en la segunda parte de este trabajo los resultados de la síntesis y la caracterización de un compuesto bio-mimético son presentados. Una de las más importantes contribuciones de esta parte, es la propuesta del uso de la clorofila como una fuente natural para obtener el ligante porfirínico para nuestro compuesto, así, la extracción de la clorofila a partir de la espinaca fue hecha y el átomo de magnesio fue extraído para generar el ligante feofitina. El proceso entero de extracción fue llevado a cabo usando técnicas cromatográficas, demostrando la composición química de los extractos en cada paso por espectroscopia electrónica. Un complejo feofitina-hierro (II) fue sintetizado y caracterizado por medio de las espectroscopias de UV-Vis y RPE, evidenciando la presencia del anillo porfirínico de la feofitina y el hierro (II) de bajo spin. La evaluación de la reactividad del compuesto frente a ácido peroxiacético fue hecha mediante un estudio cinético y espectroscopía RPE, demostrando que el PAA efectivamente reaccionaba frente al átomo de hierro causando la oxidación posterior de Fe^{II} a Fe^{III}. Desafortunadamente, no fue posible aislar un compuesto de hierro en altos estados de oxidación en este sistema inorgánico, sin embargo, el hecho de haber logrado demostrar que el compuesto es capaz de mostrar reactividad frente al ácido peroxi-acético es la base de la construcción de un sistema bio-mimético en el futuro cercano.

Palabras clave

Oxo-hierro; Biomimético; catalasa-peroxidasa; Compuesto I; feofitina; RPE; UV-Vis

TABLE OF CONTENTS

1. Introduction-Justification

1.1 General considerations about Fe

Iron is a transition metal, very abundant in the principal reservoirs on the Earth and is one of the most essential elements used by living organisms. According to the nucleosynthesis process, this metal is formed inside of stars followed by fusion reactions at high pressures and temperatures; most stable isotopes of iron are ^{54}Fe, ^{56}Fe, ^{57}Fe, and ^{58}Fe. [1] Molecular weight of iron is: 55.845 a.m.u[2]; according to its atomic number: 26, it is located in the group 8, period 4 of the Periodic Table. Electron configuration: [Ar] $3d^6 4s^2$ makes Fe^0 a d^8-species. In Pauling´s scale the iron electronegativity is 1,83; it has a melting point 1811 K and a boiling point of 3134 K. The effective ionic radii (Å) are according to spin state Fe^{2+} (ferrous state) LS 0.61 and 0.78 for HS; in the case of Fe^{3+} (ferric state) the effective radii are 0.55 LS and 0,645 HS.[3]

Interesting ductile and magnetic properties for iron compounds have been observed and exploited in technology as well as in food industry and environmental care. For instance, supplementary milky products are being constantly evaluated in Iron (Fe^{2+} & Fe^{3+}) salts type and concentration in dairy alimentation to improve the human´s health. [4] On the other hand the sanity of ecosystem also is a problematic fact, however an effective solution is for example the utilization of Fe^0 wool and a pH-dependent chemical process in the elimination of pollutant in water reservoirs that specifically are caused by solids with low solubility prevenient of TNT´s detonation used in the construction area.[5] In agreement with the previous uses mentioned before, one of the most important is the assembly of alloys based on Fe^{2+} to generate smart materials in metallurgical industry (with Sb or arsenic).[6] Special attention on the dioxygen activation by iron inorganic complexes and by very sophisticated biological systems have been taken by a lot of scientist due to the importance of such processes in several metabolic routes and in diverse applications.[7] As an introduction to this chemistry, we will revise general properties and reactivity of dioxygen.

1.2 Dioxygen properties and reactivity.

Undoubtedly, before starting to talk about the chemistry of dioxygen, we must remember the importance that dioxygen has for the existence of life on earth, we know that

air is indispensable for human life due to the participation of O_2 as electron acceptor in the respiratory chain.

Molecular orbital theory allows explain the double bond generated between two oxygen atoms in the dioxygen molecule, those covalent bonds can be described using the corresponding Molecular Orbital diagram: σ MO is obtained overlapping of two atomic 2p orbitals of each oxygen atom whereas π-MO is obtained overlapping of two atomic orbitals 2p with two pairs of electrons. The ground state of dioxygen is a triplet ($^3\square_g^-$) in which the LUMO orbital is composed by σ_{2p}^* and in the HOMO, π_{2p}^* -degenerated orbitals have two unpaired electrons that concerns the magnetic properties of O_2. Interestingly, there are two excited states with singlet multiplicity, $^1\square_g^+$ and $^1\square_g$, both cases are considered excited states due to their higher energy in comparison with the triplet state (Figure 1). Singlet forms of O_2 plays an important role in photochemical reactions in biological process and blanching power in the textile industry.[8]

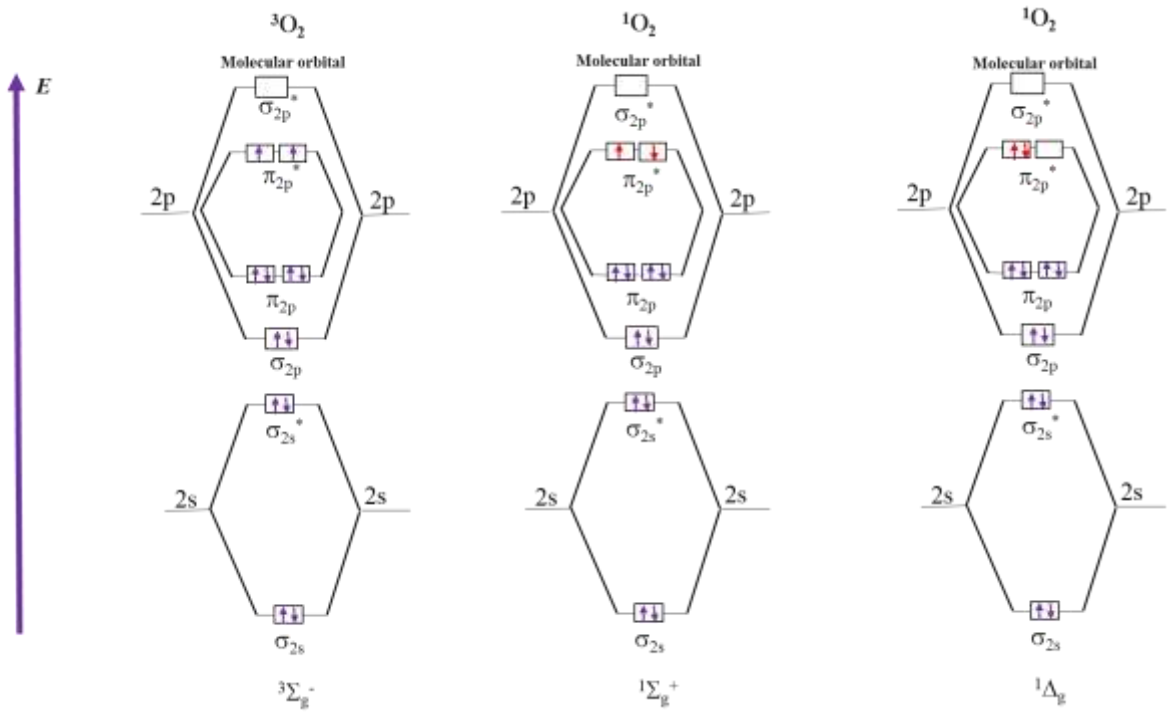

Fig. 1 Molecular Orbital Diagrams of ground state (triplet) and excited states (singlet) of O_2. Taken from Huheey.[9]

An important chemical characteristic of dioxygen is its ability to be reduced by pairs of electrons. Although less frequently, there are also cases in which O_2 is involved in mono-

electronic transfers that are of greater energy cost than transfers of electron pairs. The energetic differences between mono and bi-electronic transfer processes are revealed when the redox potentials of the different oxygen-derived species are examined. If we observe the redox potential of the O_2/O_2^- pair, it has a value of -0.05 V at pH = 0, whereas, the reduction of dioxygen to peroxide has a value of +0.695 V, which indicates that the bi-electronic transfer process is thermodynamically more favorable. (Fig. 2)

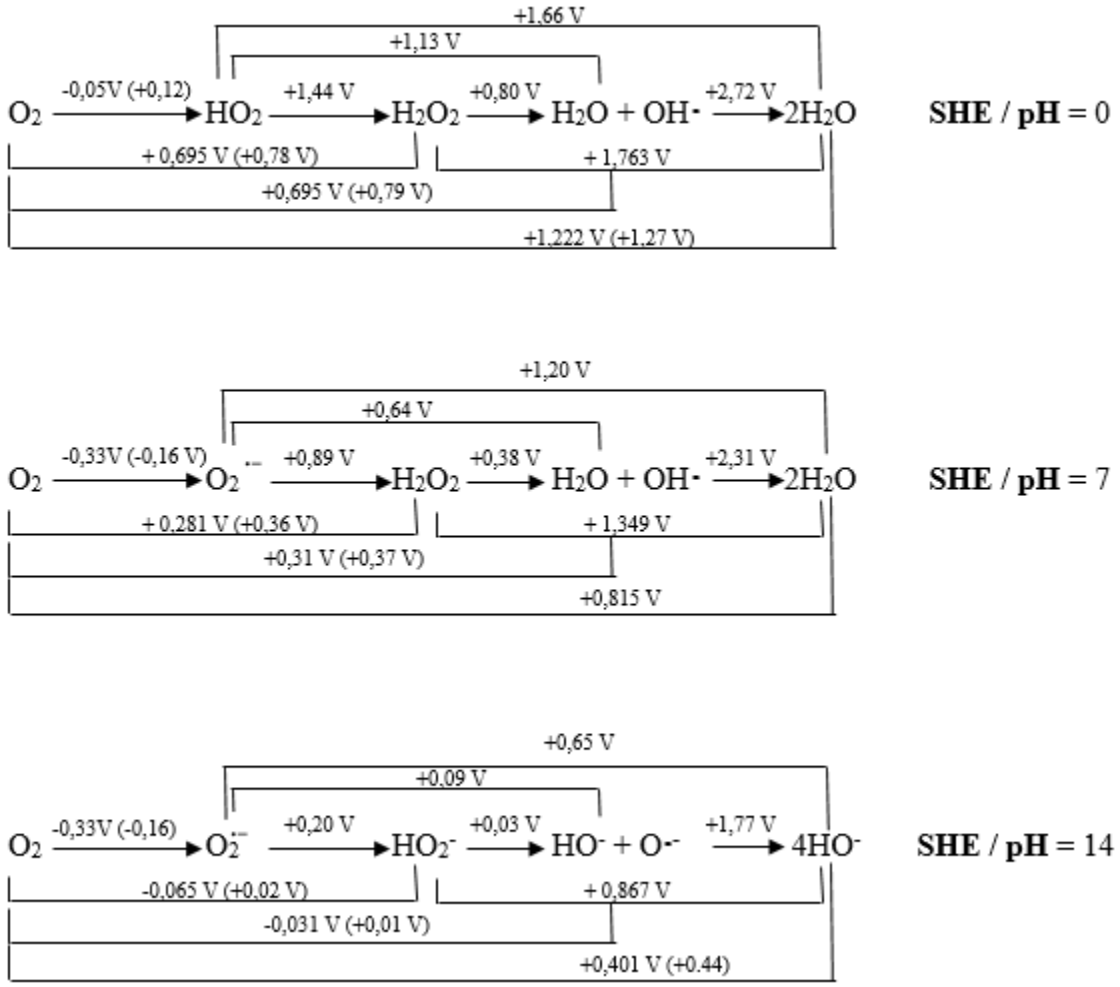

Fig. 2 General Latimer diagram for O_2 redox potentials at different values of pH. Taken from Atkins.[10] and Saucedo.[7]

In living systems as well as in chemical systems, different chemical species derived from molecular oxygen have been found; this group of species is known as Reactive Oxygen Species (ROS). Such group of ROS includes the species derived from the reduction of molecular oxygen as the superoxide/hydroperoxide radicals ($O_2^{\bullet-}/HO_2^{\bullet}$), hydrogen peroxide ($H_2O_2$) and the hydroxyl radical ($OH^{\bullet}$). Species coming from the reaction of radicals centered

on carbon with molecular oxygen: peroxyl radicals (RO_2•), alkoxyl radicals (RO•) and organic hydroperoxides (ROOH); and other oxidants that can result in the formation of free radicals, such as hypochlorous acid (HOCl), peroxynitrite ($ONOO^-$) and the aforementioned singlet oxygen ($O_2\ ^1\Delta_g$). Some authors include in this classification ozone (O_3), nitric oxide (•NO) and nitrogen dioxide ($•NO_2$) because these chemical species are sources of exogenous radicals and even nitrogen oxides can produce endogenous radicals.[7]

1.2.1 Reactive oxygen species (ROS) and their importance in catalytic cycles of enzymes.

There are chemical and biochemical reactions in which the production of ROS are relevant due to their high reactivity and damage in biological molecules such DNA, proteins, so on. However, enzymatic catalytic cycles in nature generates those byproducts as defense mechanism to the pathogen organism. Electronic Paramagnetic Resonance (EPR) spectroscopy is of great importance for the characterization of those paramagnetic species. In Fig. 3, ROS produced during reduction process of dioxygen molecule are explained in detail:

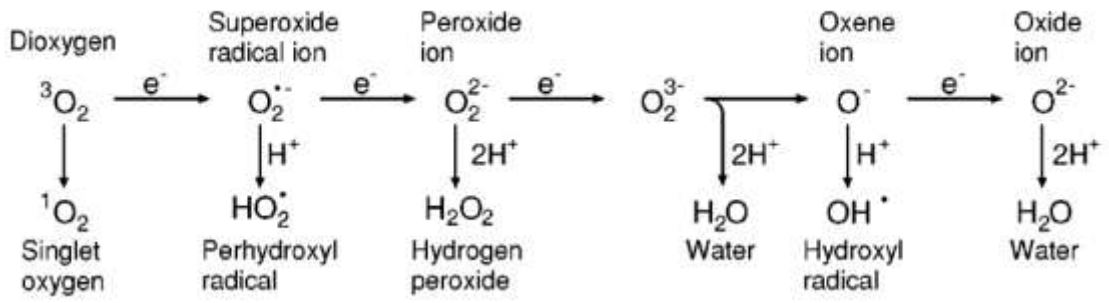

Fig. 3 Electron reduction of $^3O_2$ and ROS generation step by step. Taken from Apel and Hirt. [11]

1.3 High-valent Oxo iron compounds (Fe^{IV}=O; Fe^{V}=O)

Nature chose transition metals in order to do the hard work of redox chemistry, from these transition metals, iron plays important role in several biological processes. As we show before, the most stable oxidation states of iron are Fe^{2+} (d^6-species) and Fe^{+3} (d^5-species), we can found this oxidation states as part of the catalytic cycle of some metalloenzymes and in most of the "beaker" reactions in laboratory, however, higher oxidation states have been observed in several processes. In high valent-iron compounds, iron presents an oxidation state greater than 3 and shows a number a coordination number ≤ 6. Cristal Field Theory (Fig. 4) and Ligand Field Theory could explain octahedral field splitting of d-orbitals. In the first case, electrostatic interaction between positive charge of metallic cation and negative

from ligand, in which d-orbitals from transition metal break the degeneracy and occurs the splitting. In the case of octahedral field, there are two groups of orbitals, $\mathbf{t_{2g}}$ that is lower in energy than e_g orbital group.

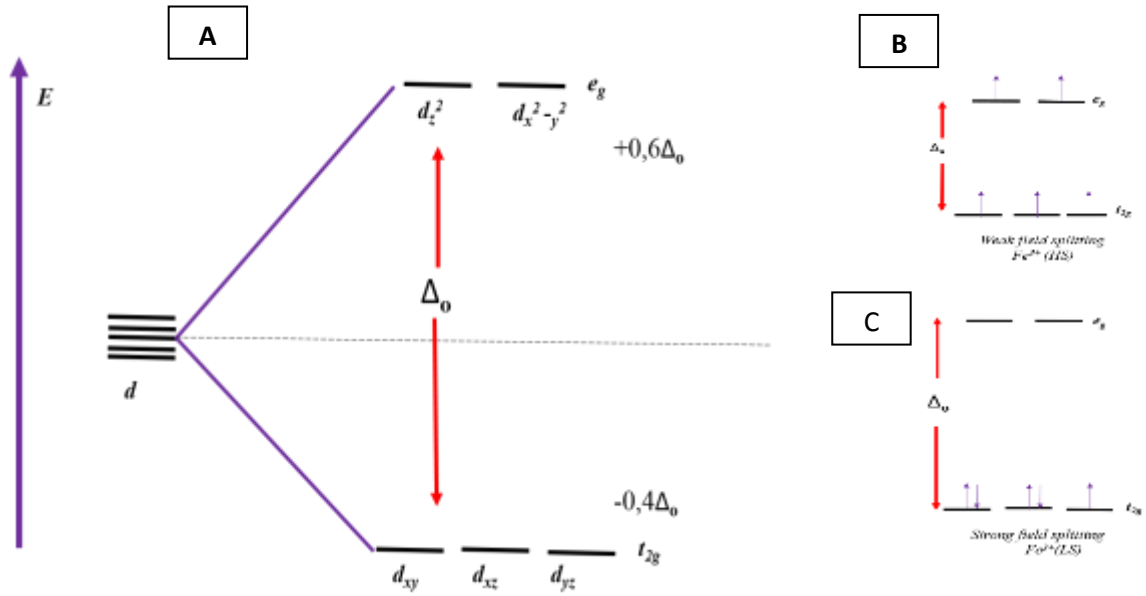

Fig. 4 Octahedral field splitting for a metal of transition series in PT. A: General splitting, B: High-spin Fe3+octahedral splitting with S=5/2, C: Low spin Fe3+octahedral splitting with S=1/2.Taken from Kenkel.[12]

On the other hand, LFT can be describe as a combination of MOT and CFT because conserve the electrostatic principles and includes organization of orbitals and interaction between metallic atom and ligand[9]. That interaction among π – orbital from ligand and d-orbitals generates a variation in Δ_O following the spectrochemical series of chemistry[10] and biochemistry (A. Thomson). Such crystal field splitting could generate LS or HS complexes (Fig. 5).

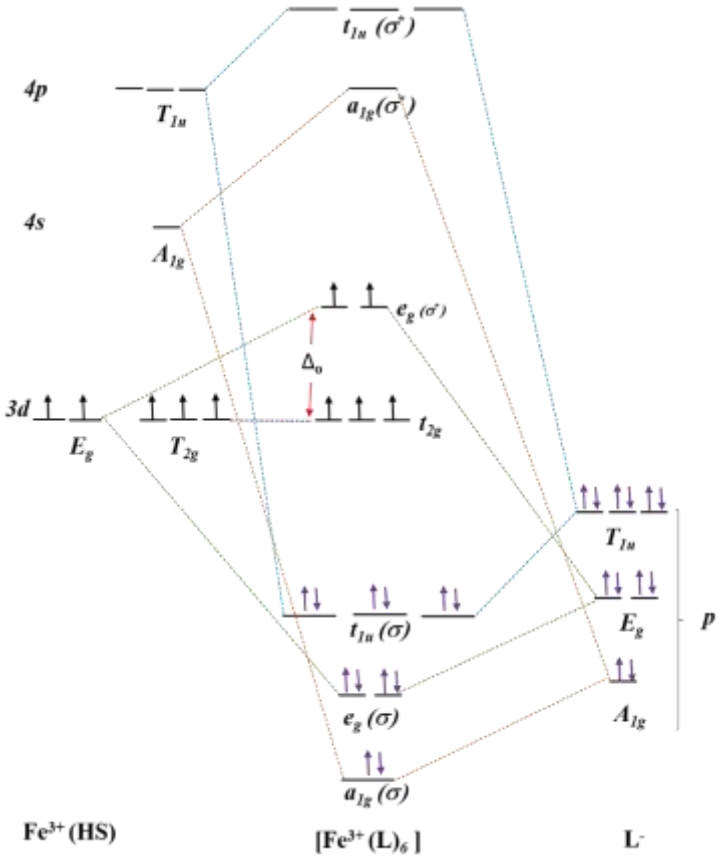

Fig. 5 Ligand Field diagram of $[FeL_6]^{3+}$. Taken from Huheey.[9]

Dioxygen molecule could be an excellent ligand due to the presence of two electron pairs in sp^3 hybrid orbitals. Coordination of dioxygen to iron as well as the redox properties of both species, makes a very interesting reactivity in the activation of dioxygen by iron and will be material of discussion in next chapter.

1.3.1 O_2 activation by iron

One of the most studied process in which high-valent iron compounds are present is in dioxygen activation in aerobic environments in nature. Atmospheric O_2 presents a thermodynamic prohibition in the first step of one electron reduction (E^0 = -330 mV), such prohibition can be sorted by two mechanisms: generation of excited singlet dioxygen and the coordination of O_2 to copper or iron. In the second case, two mechanisms for O_2 activation are possible: Inner Sphere electron transfer (IS) and Outer Sphere electron transfer (OS).[13] Outstanding efforts to determine the type of mechanism for the electron transfer from iron to oxygen in iron metalloenzymes have been performed for many years. However the mostly

of cases, the intermediates of the biological reactions are very labile and in consequence is difficult obtaining the evidence of that. In order to facilitate the understanding of such biological processes, biomimetic inorganic compounds could be synthetized and used as structural, spectroscopic or functional models.

Since inner sphere electron transfer is most common mechanism to activate dioxygen by iron, and due to this issue is the main topic of this thesis, my efforts will be centered on the discussion of this type of mechanism. Then, in the next sections, relevant examples of dioxygen activation in biological and synthetic compounds *via* inner sphere mechanisms are presented.

1.3.2 High-valent Oxo iron compounds in biological systems

A structural characteristic that allows classify the mechanism of the electron transfer in metalloproteins that activates O_2 is the heme moiety, thus, in the literature is very common the classification in heme and non-heme groups.[14]

1.3.2.1 Non-heme active sites in metalloenzymes

In the case of non-heme metalloproteins, we found versatility in the coordination environment on the iron center, a good example of such versatility is the case of the penta-coordinated non-heme metallic center in the protocatechuate 3,4-dioxygenase enzyme of *Pseudomonas aeruginosa*. This enzyme was crystallized and the 3D structure reveals a trigonal bipyramidal geometry for iron center. Four of the ligands corresponds to amino acids and in an equatorial position, a hydroxide was confirmed using EXAFS technique.[15] Sophisticated reaction mechanism for the cleavage of protocatechuate (3,4-dihydroxybenzoate) to □-carboxy-*cis,cis*-muconic acid was found, spectroscopic results in combination with X-Ray diffraction and the mentioned EXAFS results demonstrate that dioxygen attacks firstly the organic coordinated substrate instead the iron center, this is the reason why iron(III) is conserved during the catalytic cycle. Once the intermediate Fe-O-O-C is formed, cleavage of dioxygen molecule is easiest and oxygen transfer to form the diacid occurs (Fig. 6).

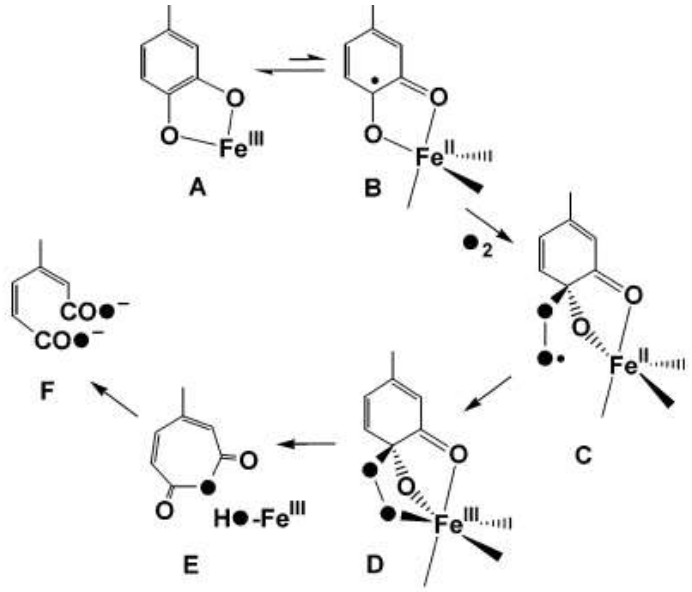

Fig. 6. Reaction mechanism for the protocatechuate cleavage in protocatechuate 3,4-dioxygenase enzyme. Taken from Costas[15] and Denisov.[16]

1.3.2.2 Heme active sites in metalloenzymes

Extensive studies around Cytochrome P450 (CytP450) reaction mechanism and the use of several spectroscopies, reveals high-valent oxo iron compounds as key intermediates of the reaction. Another oxo-iron species as Fe^{3+}-OO- (ferric superoxide) with a characteristic Raman signal centered in 1140 cm^{-1} was identified. Cytochrome P450 (with shoret in λ_{max} = 450 nm) has been object of extensive studies and is considered a model of O_2 activation by heme enzymes. Generation of Cyt-P450 mutants as well as catalytic activity evaluation followed by long-wave length X-rays experiments allows the capture[16] of some oxo-iron intermediates. One of these is the so-called Compound I in which a ferryl oxo-iron moiety coupled to a cationic porphyrin $Fe^{+4}=O^{+\bullet}$, which plays a critical role in heme dioxygen activation as intermediate in the catalytic cycle of several enzymatic reactions and not only on Cyt-P450. One-year later, another intermediate was isolated from reaction of H_2O_2 with cyt-P450 from the thermophile *Sulfolobus solfactaricus*. Such intermediate contains $Fe^{+4}=O$ in a neutral molecule named Compound II (Fig.7). The characterization of such intermediates have been made by using EPR, Raman and UV-Vis.[17]

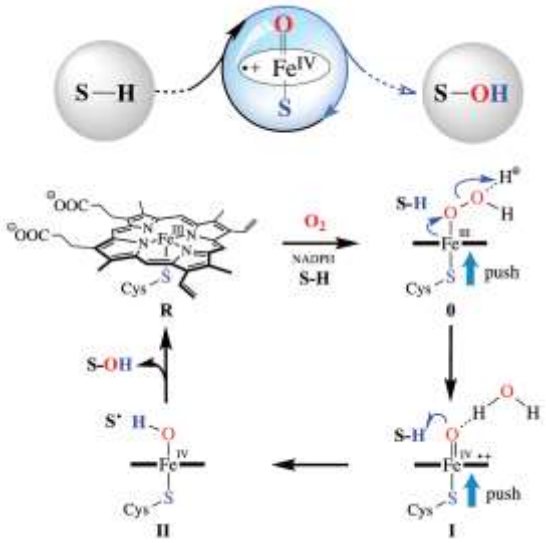

Fig. 7. Catalytic cycle of enzymatic reaction in Cytchrome P450. Taken from Groves.[18]

Binuclear cofactors present in metalloenzymes such as soluble methane monoxygenase (sMMO) and non-heme ferritin have make possible the identification of a peroxodiiron, known as R2 intermediate, which during activation of O_2 reveled in Mossbauer spectroscopy experiment parameter that correspond to those suggested species (δ = 0.55–0.68 mm s^{-1}). During the catalysis a dioxygen molecule is activated given a radical peroxo in which two iron atoms are oxidized to 3+, then this radical (R2) make a second oxidation of a tryptophan residue (W48) related to redox process of deoxyribonucleotides and form the intermediate X which present one atom of Fe^{3+} and other Fe^{4+} in the binuclear cofactor.[19]

Study about limiting-step in the reaction mechanism of hydrophobic proteins such as lipoxygenase has allowed revel high-valent Fe^{IV}=O intermediates though outer sphere mechanism, the electronic transference from its hydrophobic pocket where are amino acids residues has been studied using variants of wild type protein. Those experiments were analyzed using Xray crystalline structure and Solvent deuterium kinetic technique gave more evidence that put high valent oxo-iron intermediate in limiting-step of reaction. This is a human enzyme that transforms fatty acids into leukotrienes which are the latest advance in curative medicine of respiratory diseases and makes its reaction mechanism of great interest.[20]

As we saw before, intermediates of the enzymatic reactions are too difficult and hence, the reaction mechanisms are a really hard work to do for the chemists and biologist, thus in an effort to help the elucidation of such mechanisms, inorganic models with different levels

of mimicry have been developed. In the next section, some examples of such biomimetic compounds are described.

1.3.3 High-valent Oxo iron compounds in inorganic systems

An interesting example of inorganic oxo-iron complex was found in the attempt to synthetize a biomimetic of Photosystem I, in which a ferrous inorganic compound $[((N4Py)Fe^{II}(NCMe)]^{2+}$ reacts with $Ce^{IV}(NH_4)_2(NO_3)_6$ which is used often as oxidant in artificial oxidation of water in outer sphere electron transfer mechanism. In the case of this work, surprisingly, an inner sphere product is obtained, Fe^{IV}–O–Ce^{IV} in a irreversible reaction. The characterization of such intermediate was made using Raman spectroscopy in which the shifting (822 cm^{-1}) $\nu_{Fe=O}$ vibration is remarkable. (Fig.8).[15]

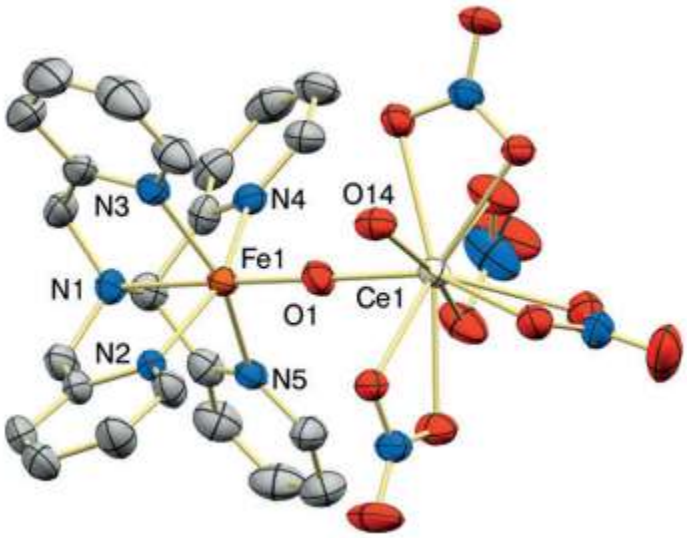

Fig. 8 Intermediate isolated that mimic an inner sphere high valent oxo iron compound from reaction mechanism of biological Photosystem I.$[(mcp)Fe^{IV}(O)\ (\mu\text{-}O)Ce^{IV}(NO_3)_3]^+$. Taken from Draksharapu. [21]

Classic examples of synthetic oxoiron complexes are TMC-iron compounds (TMC =1,4,8,11-tetramethyl-1,4,8,11-tetraazacyclotetradecane), eg. $[Fe^{IV}(O)(TMC)(CH_3CN)]^{2+}$ where inspired in non-heme iron intermediate presents thermal stability, high yielding and a pale green color, in fact, this type of synthetic oxoiron complexes were the first to be isolated an characterized unambiguously (Fig. 9). [22,23]

Fig. 9. Crystal structure of $[Fe^{IV}(O)(TMC)(CH3CN)]^{2+}$ .Taken from Rohde. [23]

An excellent example of a functional inorganic model of heme-like dioxygen activation is the case reported by Bhakta and coworkers .[24] In this work, the synthesis of an iron porphyrin compound with a modification in the aromatic ring allows establish a second coordination sphere interaction that can stabilize intermediates like Compound I.

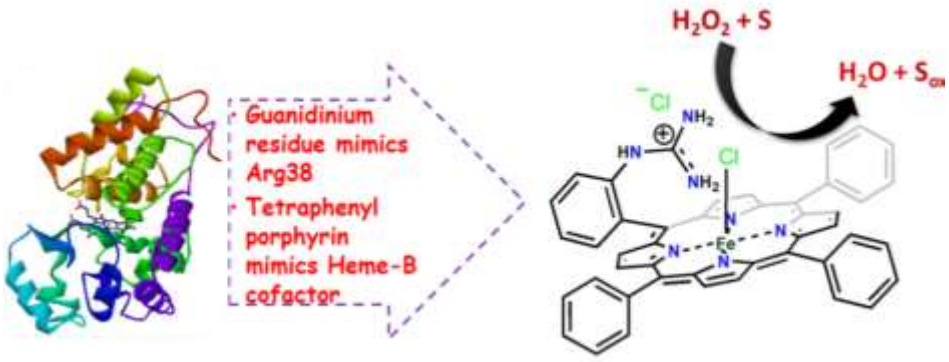

Fig. 10. Functional peroxidase like biomimetic iron-porphyrin compound. Taken from Bhakta. [24]

In the case of peroxidase enzymes, the reaction mechanisms consist in the formation of ferryl intermediate (Compound I) by the redox reaction of O_2 and Fe^{III}_{heme} mediated by the acid-base catalysis of distal amino acids like Arg and His. Once the Compound I is formed and stabilized by the same Arg through hydrogen bond interactions. Thus, in this work the complex o-Monoguanidinotetraphenyliron(III)-porphyrin(Fe^{III}Cl-MARG) contains the guanidine like substituent works as stabilizing of the artificial ferryl intermediate. Surprisingly, the peroxidase like activity using different reductant agents were performed, and the kinetic results shows a comparative results with the enzymatic ones (Fig. 11).

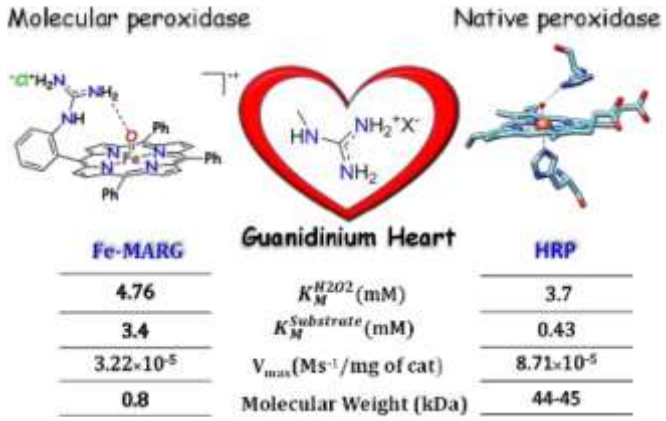

Fe-MARG		HRP
4.76	K_M^{H2O2}(mM)	3.7
3.4	$K_M^{Substrate}$(mM)	0.43
3.22×10^{-5}	V_{max}(Ms^{-1}/mg of cat)	8.71×10^{-5}
0.8	Molecular Weight (kDa)	44-45

Fig. 11 Mikaelis-Menten kinetic results of Fe-MARG compound compared with horseradish peroxidase. Taken from Bhakta.[24]

1.3.4 Special case of study. Catalase-Peroxidase of *Neurospora crassa*.

The enzymatic model that works as inspiration for the present document is the bifunctional catalase-peroxidase (CAT2) enzyme, isolated from the fungus *Neurospora crassa*. This cytosolic protein is a homodimer of 170 kDa (monomer 83.4 kDa) whose aminoacidic sequence is conserved in comparison to others catalase-peroxidase enzymes founded in bacteria and fungus. CAT2 active site is composed by a heme type *b* group which has a pentacordined structure in which Fe^{3+} is bounded to an axial histidine, close to the heme *b*, a prosthetic organic cofactor given by the aminoacidic triad or covalent adduct M-Y-W is located.[25] Such enzymatic engineering is founded in all the catalase-peroxidases[26] no matter the source of the protein (Fig. 12). The access to heme group by part of substrate is mediated by two amino acids: Asp120 and Arg 426 that are in the end of the entrance channel and gives the selectivity to the CAT2 respect to reactant size during the catalytic activity.

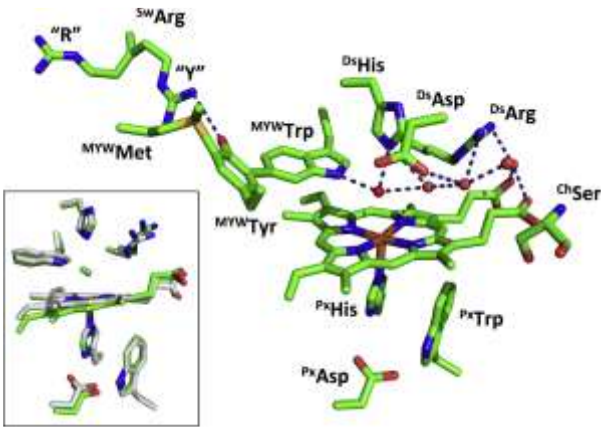

Fig.12. Active site in catalase-peroxidase enzymes. Taken from Njuma. [26]

Eventually, the bifunctional catalytic activity of CAT2 can be described as reduction of H_2O_2 to produce O_2 and $2H_2O$ in the presence (peroxidatic) of an external reductant or in the absence (catalase) of such reductant. In the case of catalase activity, in which two molecules of substrate are present as electron donors and promotes the dismutation of H_2O_2. The reaction mechanism for catalase and peroxidase activity is the same in the first tree steps, when the cofactor enters in contact with H_2O_2 molecule a covalent bond is formed between Fe^{3+} and O-OH. Thus, oxidation of Fe^{3+} to Fe^{4+} followed by realizing a water molecule is achieved. Then, two electrons are oxidized one from the iron of heme and other from any amino acidic residue given as a result the well-known cationic radical Compound I {Fe^{IV}=O $por^{+\bullet}$} which subsequently evolves to Compound I* in which the free electron centered in the cationic porphyrin, is transferred to adequate amino acids located in the peripheral of the active site. This reaction intermediate has been allowing the study of electronic and spectroscopic characteristic of some metalloproteins which goes through formation of high valent oxo-iron compounds[27] in its catalytic cycle (Fig. 13).

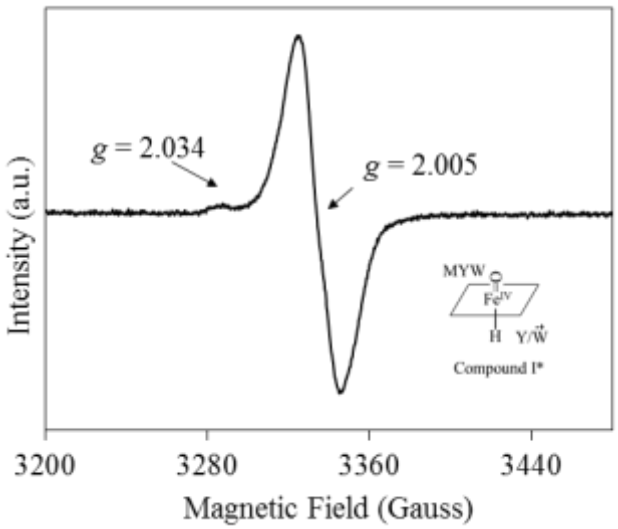

Fig. 13. EPR spectrum of the ferryl intermediate Compound I* in CAT2 catalytic cycle. Taken from Vega. [27]

As we saw before, labile intermediates makes the work very hard for the dioxygen activation and the use of several spectroscopic techniques to elucidate the reaction mechanisms. In the next section, short review on EPR is presented.

1.3.5 Electronic paramagnetic spectroscopy (EPR)

Due to the importance of Electronic Paramagnetic Resonance spectroscopy to characterize paramagnetic species founded as labile intermediates and in resting states or reactants in different mechanisms of activation of dioxygen by iron, a little description will be presented below.

EPR is a spectroscopic technique in which the absorbance of microwaves by an organic, inorganic, biological or synthetic molecule with unpaired electrons and odd spin value can be detected. During the experiment in EPR, we perform a magnetic field sweep and in the resonance condition (Eq. 1), an excitation that changes the spin state of free electron occurs (Fig. 14).

When magnetic field is applied a splitting of two states of energy are generated, one on the direction of the magnetic field $m_s = +\frac{1}{2}$, and other against with $m_s = -\frac{1}{2}$. The transition of spin state energies is measured by Eq. 1.

$$\Delta E = g\square H \qquad \text{(Equation 1)}$$

Where: g: is the giromagnetic constant for one electron (2, 0023192778 ≈ 2.00); β: is the electron Bohr magneton (BM) and H is the external field applied.[12]

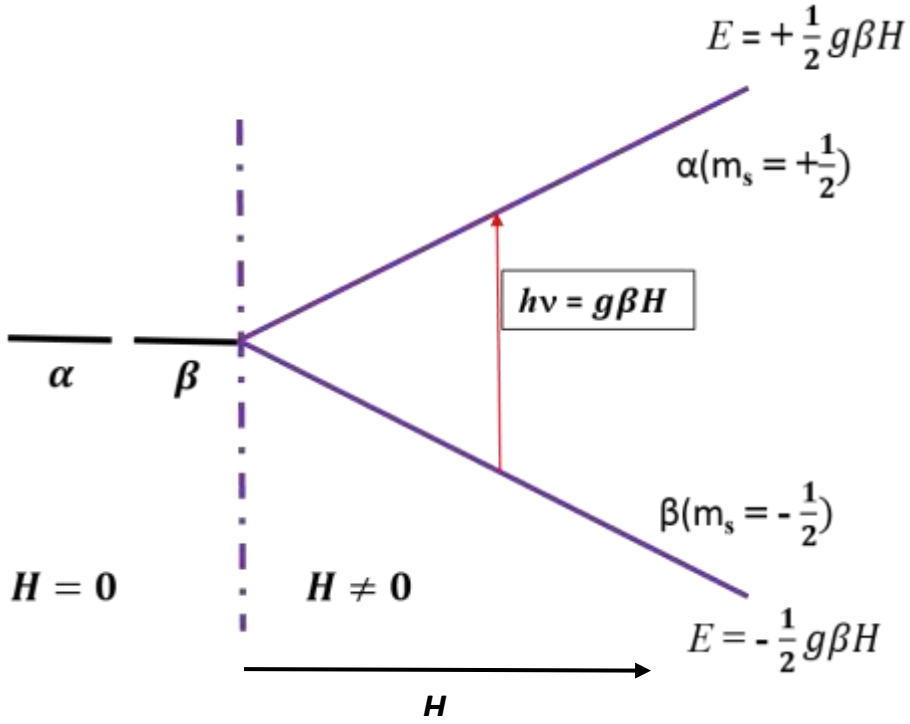

Fig. 14. Splitting of energetic levels in Electronic Paramagnetic Resonance. Taken from Drago[12] and Solano.[28]

The more common frequency used in EPR are 9.5 GHz (X-band) and 35 GHz (Q-band), 3400 gauss and 12 500 gauss respectively. Normally, tubes depend of sample type; it must be quartz of tubular or planar shape; eventually, solvent used is selected according to dielectric constant for avoiding the microwaves absorbance that creates noise in signals.[12] Sample (10^{-3}M – 10^{-4}M approximately in concentration) is frozen at low temperatures (around T = 10 K) using N_2 and He in liquid state. Spectrum is recorded with its respective second derivative in order to reduce errors in g-value determination. One unpaired electron can produce three kind of symmetry in spectrum: spherical, axial and rhombic which will be unique for that sample.

Biological and synthetic samples are part of the extensively studied compounds by EPR, among this, organic radicals, enzymatic metallic cofactors with unpaired electrons, coordination compounds that mimic heme and non-heme active sites have been studied.[29]

This EPR device is able to be adaptable to sample in any aggregation state, for example, a research on tridentate and monoprotic Schiff bases used to be coordinated to Iron atom has confirmed the inactivity of Fe^{2+} species. However, X-band EPR experiment using a crystalline sample at 70 K has elucidated the remarkable axial signal with g = 2.14 and g = 1.94 for metallic center Fe^{3+} Low Spin (LS). Experiment at 170 K was repeated, an LS-HS intermediated state was assigned which signals are g = 4.64 for Fe^{3+} HS and Fe^{3+} LS a value of g = 2.06.[30] Additionally, another study at room temperature has revealed a broad peak characteristic of Fe^{3+} of High Spin (HS) with S= 5/2 a value of g = 5. 25 at room temperature and axial symmetry that define ferric LS at g = 2.20 and 1.96.[31]

2. Problem Statement

As we saw in the introduction, high-valent oxo-iron intermediates generated by inner sphere electron transfer mechanisms are present in most of the reaction in which dioxygen activation is involved. Both biological (enzymatic) and inorganic (biomimetic) systems are difficult to study and not all the mechanistic details are revealed so far. In an effort to contribute with results to clarify those reaction mechanisms, the present work will show the study of the reaction mechanism of D120A variant of CAT2 from *Neurospora crassa* and the synthesis, characterization and reactivity of an inorganic synthetic biomimetic based on a porphyrin derived of chlorophyll with an iron center.

3. Objectives

General Objective

The main goal of this work is the isolation of high-valent oxo-iron (Fe^{IV}=O) intermediates presents in the reaction mechanism of dioxygen activation by a biologic system (CAT2_D120A) and the synthesis of an inorganic model of iron with a chlorophyll-derived ligand to mimic the biologic system through oxo-iron intermediates.

Specific Objectives

- Construction of the CAT2_D120A variant as well as the purification of such enzyme.

- Characterization of CAT2_D120A resting state with UV-Vis and EPR spectroscopies and evaluation of the effect of the mutation on the catalase or peroxidase function.

- Generate Ferryl (Fe^{IV}=O) intermediates artificially by a reaction of the enzyme with PAA and perform the characterization of such intermediates.

- Isolation of a chlorophyll derivative from a natural source and perform the synthesis of an iron complex with such ligand in order to generate a heme-like synthetic compound.

- To evaluate the reactivity of the synthetic model against dioxygen or some reactive oxygen species to establish a mechanistic correlation with the biological system (CAT2_D120A).

4. Materials and Methodology

4.1 Reactants and equipment

Reactants

Biological System CAT2_D120A	Inorganic System- Fe-pheo
NaH_2PO_4 (99%.Sigma-Aldrich). NaCl (99.5 %.Sigma-Aldrich). Imidazole (99%. pH=10.Sigma-Aldrich) Hemin (from bovine 90%.Sigma-Aldrich) IPTG (Invitrogen TM) Nucleasas (Invitrogen TM) Ni-NTA resin (QIAGEN). β-mercaptoethanol (Thermo Scientific TM) Commasie Brilliant Blue (Sigma-Aldrich). Polyacrylamide (Sigma-Aldrich) SDS (98.5%. Sigma-aldrich) $K_3[Fe(CN)_6]$ (99% Sigma-Aldrich) $FeCl_3$ (98%. Sigma-Aldrich) o-dianisidine (95%. Sigma-Aldrich) Sodium dithionite (Merck KGaA) KCN (96%. Sigma-Aldrich)	Commercial spinach Silica gel 60 Na_2CO_3 (99%. Sigma-Aldrich) Acetone (99.7 %. J.T Baker) Petroleum ether (distilled recovery) Hexane (98%. Fisher scientific) Ethanol $FeCl_2 * 4H_2O$ (98%. ReagentPlus) $CoCl_2$ (98% Sigma-Aldrich) Whatman PTFE membrane filters. 1.0um, 25 mm, 50/pk (Sigma-Aldrich)

Equipment of laboratory

- Agilent 8452 diode array UV-Vis spectrophotometer.
- UV-Vis spectrophotometer Nanodrop 2000c
- Specord S600 Analitik Jena diode array spectrophotometer
- EPR: ELEXSYS E500 spectrometer equipped with a standard Bruker ER4123SHQE X-band cavity resonator at a frequency of ≈ 9.40 GHz.

4.2 High valent oxo-iron species in CAT2_120A enzyme

4.2.1 Expression of CAT2_D120A mutant

Molecular biology engineering developed previously for the heterologous expression of wild type catalase-peroxidase of *Neurospora crassa*[25,32] was used for D120A mutant expression. *Escherichia coli* bacteria was used to express the catalase-peroxidase gen, the strain M15/pREP4 (kanamycin resistant) transformed with pD120A plasmid (ampicillin resistant) was pre-cultured during 16 hours overnight in 100mL of LB medium with ampicillin (100ug/mL), at 37°C and 200rpm. The pre-culture was transferred to 1L of LB-ampicillin at 37°C, 200rpm for 1 hour until optical density $O.D_{600} = 0.5$, then the media was

induced with IPTG (1mM) and 3mL of hemin (60mM, pH: 9.3) and incubated for 6 hours (sterile conditions). After that, the bacterial cells were collected by centrifugation at 4500rpm (JA10 BECKMAN Rotor) and 4°C. The pellet was re-suspended in 20mL of lysis buffer (50mM NaH_2PO_4, 300mM NaCl, 10mM imidazole, pH: 8.0). Disruption of cellular membrane was made using lysozyme stock solution (100mg/mL), adding aliquots of 30 mL to re-suspended cells in sterile falcon tubes (lysozyme was added 10uL per 1mL of suspended cells) at 4°C in ice-bath. Then lysed cells was treated using liquid nitrogen of each falcon tube and treated with a heat-shock of 42°C hot-bath three times. After, 5ul of DNAsa I (10mg/mL) and 5□L of RNAasa A per milliliter of cells were added during 1 hour 30mins at 37°C until viscosity was not appreciable. Finally, protein fraction was recovered using centrifugation at 9000rpm for 15min at 4°C, then the supernatant was transferred to new falcon tubes and protease inhibitors Sigma Aldrich (10mM) $1mL^{protease}/mL^{protein}$ and 1uL of phenylmethanesulfonyl fluoride PMSF were added.

4.2.2 Purification of CAT2_D120A mutant

The isolated protein was incubated with 5-7 mL of Ni-NTA (QIAGEN) resin for 12 hours at 4°C in constant stirring. Column of 15cm large and 1,5cm of diameter was loaded with the Ni-NTA resin and protein. Packed resin was washed with 25mL of lysis buffer, 100mL of wash buffer (50mM Na_2PO_4, 300mM NaCl, 20mM Imidazole, pH:8) and 40mL of elution buffer (50mM Na_2PO_4, 300mM NaCl, 250mM Imidazole, pH:8.0). The elution buffer of the protein was followed by the characteristic red color taken from their oxidized-heme *b*. Protein fractions were collected in a tube and concentrated using an Amicon 30KDa (Milipore) using phosphate buffer (Na/K 50mM, pH:7.8). [25]

4.2.3 Characterization of CAT2_D120A.

4.2.3.1 Electrophoresis

Sodium dodecyl sulfate polyacrylamide gel electrophoresis (SDS-PAGE) method was used for protein separation as follows: Mini-PROTEAN Cell equipment at 75 V for 15 min, followed by 200V for 50 min which was carried out using 8% polyacrylamide gel and running buffer (3.3 g of trizma base, 14,4g of glycine, 1L of distilled water and 1g of SDS, pH: 8.3). 30 □g of each protein were loaded using *β-mercaptoetanol* previously boiled at 100°C during 15-20min, then the gel was stained with Commasie Brilliant Blue (Sigma-Aldrich).

Native PAGE was made with the same equipment, but using a running buffer without SDS. The native buffer (Thermo Fisher Scientific) was added 1□L for every 5mL of protein. Zymography in native PAGE was used to evaluate the catalase and peroxidase activity; catalase zymogram was carried out using methanol (5%) during 5 mins, then washing twice the gel with distilled water and incubating with hydrogen peroxide (10mM) during 5 mins. Gel washing was repeated with distilled water and then, an oxidation reaction was performed using 30mL $K_3[Fe(CN)_6]$ (2%) followed by $FeCl_3$ (2%) in order to revel the catalase activity.[33] Peroxidase activity was fixed incubating the gel in 30mL of sodium acetate buffer (50mM, pH: 6) with o-dianisidine (0,5 mM) as external reductant and hydrogen peroxide (0,1mM) until yellow bands appeared. [34] Both activity gels were scanned and stored in special waste of polyacrylamide.

4.2.3.2 Electronic spectroscopy of D120A resting state

The Reinheitszahl value was determined using UV-Vis absorbance spectra of CAT2_D120A in phosphates buffer (50mM, pH=7.8, T=25°C, blank: phosphates buffer), A_{soret}/A_{280} ratio was determined using a NanoDrop 2000c (Thermo Scientific) UV-Vis spectrophotometer with a quartz cuvette (1 cm optical path).

The redox potential of the mutant was determined by the procedure reported by Dutton.[35] UV-vis spectra was determined with an Agilent 8453 diode array spectrophotometer, a special homemade quartz cuvette for spectro-electrochemical experiments equipped with two arms for in/out of $N_{2(g)}$ continuous flux and a body to couple a redox electrode. The redox potential was measured using a platinum electrode with Ag/AgCl as reference electrode. Previous to the spectro-electrochemical experiment, a calibration of the electrode was made using 5mL of a saturated solution of quinhydrone (E_m = +280.3 mV/NHE). After ensuring the experiment conditions, the blank used was phosphates buffer (pH=7.8), the samples (10^{-4}M) in phosphates buffer, pH: 7.8 was poured in cuvette, it was bubbled with N_2 during 30 minutes. The enzyme sample was enriched with several quinones (20uL of each one) as redox mediators. Final concentration of every quinone added was 50mM in DMSO. For this experiment, quinones used were: duroquinone (E_m =+50 mV); menadione (E_m = 0mV); phenazine methosulfate PMS (E_m = +80 mV); Phenazine ethosulfate (E_m = +55 mV); 2-hydroxi-1,4-naftoquinone (E_m = -145mV). Redox

titration of D120A was performed under argon atmosphere adding aliquots of 20-30 μL of sodium dithionite and recording the redox potential changes each 10-15 mV.

4.2.3.3 Determination of the Spin State of iron in CAT2_D120A

Spin state determination of Fe^{3+} in heme cofactor was performed using the resting state of D120A, 200uL of the enzyme (10^{-4}M), pH=7.8 phosphates buffer at T=22.5° in a quartz cuvette, 10□L of KCN (10^{-1} M) solution[36] were added and spectrum was recorded after 60 min using NanoDrop 2000c.

4.2.3.4 Electronic spectra of Compound I

Oxo-ferryl intermediate formation was performed with the addition of 4uL of peracetic acid (PAA 0,1M final concentration) in 200μL of the enzyme following experimental process in literature.[37] Electronic spectra of the reaction products were determined using NanoDrop 2000c at 4°C (peltier controlled), an acetone cold bath was used to cold the reactants before the measurements.

4.2.3.5 EPR of CAT2_6H. Resting state and labile intermediates

Aqueous solutions of CAT-2 in concentration of 10 mM in 0.01 M phosphate buffer (pH = 7.0) were used, 150 uL of the mixture were placing in an EPR quartz tube of 5 mm of outer diameter, the tubes with samples were immersed directly in liquid nitrogen for storage. For the EPR measurements ELEXSYS E500 spectrometer equipped with a standard Bruker ER4123SHQE X-band cavity resonator at a frequency of ≈ 9.40 GHz was used. The next spectrometer parameters were used as standard: microwave power, 2.0 mW; modulation amplitude: 0.1 mT; modulation frequency: 100 kHz. For the low temperature experiments a Bruker ER4131VT cryostat for 100-180 K and a liquid helium cryostat ESR 900 (Oxford Instruments) for 10 K were used. [27]

4.3 High valent oxo-Iron complex synthesis in bioinorganic system

4.3.1 Isolation of chlorophyll derivative ligand

The tetra pyrrole ring heme like present in the structure of chlorophylls and their derivatives such as pheophytins and chlorophyllides has served as inspiration to synthetize an inorganic model of heme metalloproteins. Thus, prime material was commercial spinach, extraction was made pouring 10g of spinach, 1g of Na_2CO_3 and 50mL of acetone in a mortar during 10min at room temperature. First filtrate at vacuum system using a Whaltman filter paper N°1. The solid fraction (rest of plant) was pour again in mortar adding 25mL of acetone

(three times it was repeated). Acetone phase was pour in a sep-funnel and 25mL of petroleum ether (PE), it was gently mixed and finally 50mL of distilled water were added in order to drain the chlorophylls and derivatives in petroleum phase. Finally, the organic phase was stored at T= 20°C.[38] Separation of chlorophylls derivatives from another pigments was made using a purification column of silica gel 60 (solid phase) packed adding 50mL of acetone, and an eluotropic series Hexane 6: Diethyl ether 3: Acetone 2. Fractions were collected in labeled test tubes covered with aluminum foil respectively to avoid oxidation reaction. Confirmation of presence of chlorophylls derivatives using UV-Vis spectrophotometer following the soret-band and Q-band respectively, also thin layer chromatography for each test tube were reveled using eluotropic series Hexane 6: Diethyl ether 3: Acetone 2, using a UV-light chamber and iodine chamber. [39]

4.3.2 Fe-pheo synthesis

Qualitative chemical reaction was carried out using Fe^{2+} and Co^{2+} ions and chlorophyll derivative structure: pheophytin. In this sense, pheophytinization of 10mL chlorophyll crude extract was carried out adding concentrated chloric acidic acid during 2 hours at 22 °C. Then the metal-pheophytin complexes were prepared by refluxing[38] a three temperatures: 25°C , 40C° and 60°C, using iron (II) chloride tetra hydrated ($1{,}3 \times 10^{-3}$ M) and cobalt(II) chloride hexahydrate ($1{,}3 \times 10^{-3}$ M) in their respective acidic solution. Ascorbic acid (10mg) was added to avoid the action of oxygen in the structure. The reflux ended when olive green color was observed in the case of Fe^{2+}-pheo and turquoise color for Co^{2+}-pheo.

4.3.3 UV-Vis spectrophotometry characterization of the Fe^{II}-pheo complex

Agilent 8452 diode array spectrophotometer was used to characterize the Fe^{II}-pheo complex. In the case of the ligand, comparative analysis of free ligand against the complex according to the shifting of soret-band and Q-band was made. Each spectrum was measured using blank acetone: distilled water (9:1) at room temperature.

4.3.4 Reactivity of the inorganic Fe^{II}-pheophytin complex against PAA

In order to evaluate the ability of the Fe^{II}-pheo complex to activate dioxygen derivatives, a reaction between the complex and peroxiacetic acid was performed. A follow-up of the reaction progress by measure disappearance of the absorption in 395 nm characteristic of free ligand was made. This kinetic experiment was temperature controlled (25 ºC) with a peltier and mixing complex (2×10^{-4} M) and PAA (2×10^{-4} M) in water. Changes in the electronic spectra were measured every 0.1 sec during 5 sec.

After the reaction was complete, EPR of the final product was taken at room temperature as follows: aqueous solution of the final mixture in concentration of 0.1 M was used, 150 uL of the mixture were placing in an EPR quartz tube of 5 mm. The spectrometer described above was used in the next conditions: microwave frequency, 9.8 MHz (X-band); microwave power, 2.02 mW; modulation amplitude: 0.1 mT; modulation frequency: 100 kHz.

5 Experimental Results & Discussion

Mainly, the present section consist of two parts in which relevant results of the studies about high-valent oxo-iron intermediates of biological and chemical systems are presented. In the first part we describe the biological model CAT2 was chosen to be studied due to the relevance of intermediates in the reaction mechanism during oxygen activation; obtaining of CAT2 variant goes under expression procedure in an engineered *E. coli* host and its respective purification, quantification and characterization. Eventually, in the second part the synthesis of a heme-inspired biomimetic trough extraction, purification and isolation of tetra-pyrrole ring of chlorophyll derivative.

5.1 CAT2_D120A variant as biological system of study

The biological model used to study biological high-valent oxo-iron intermediates is a variant of CAT2_WT which is a homodimeric (170 kDa) bifunctional metalloenzyme showing peroxidase and catalase activity. In the active site of CAT2_WT we can find a complex engineering of cofactors in order to do the work of a catalase and peroxidase with the same efficiency than mono-functional enzymes. Catalytic center of such machinery is occupied by a Fe^{3+} heme-*b* as well as an organic cofactor composed of the amino acid triad Methionine-Tyrosine-Tryptophan and a set of distal and proximal amino acids located around the heme and essential for the catalysis (Fig.12). In distal positions, some amino acids appear, but one of the most important is aspartate. Thus, this study consists in the construction of the variant CAT2_D120A, in which aspartic acid number 120 in distal position is substituted by an alanine amino acid in order to evaluate their influence in the generation of oxo-iron intermediates, i. e., in the catalytic cycle of the enzyme.

5.1.1 Expression and inoculation of CAT2_D120A

CAT2_ D120A gene of *N. crassa* fungus was introduced in *E. coli* cells. Characteristic colonies with a brilliant-amber color were obtained, after 16 hours those turned on opaque amber color which indicated the growing of bacterial cells showing an optical density OD_{600} = 0.48. In fig. 15, physical characteristics of *E. coli* colonies with D120A plasmid and their later inoculation in liquid ampicillin-LB medium is presented.

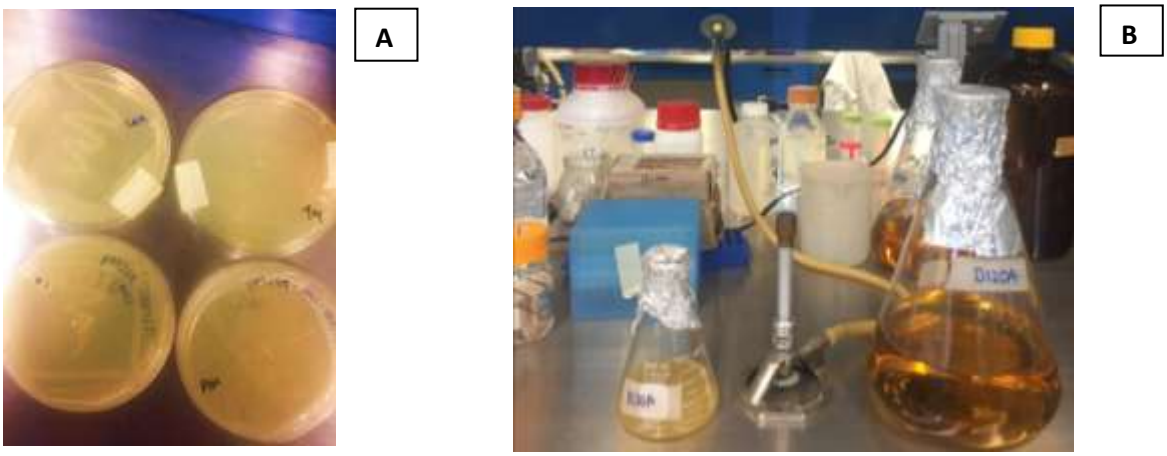

Fig. 15. CAT2_D120A expressed into engineered *E. coli* cells.

5.1.2 Purification using Chromatography of Chemical Affinity

The strategy of purification is centered on the use of the 6-histidine tag to interact with a Nickel resin by chemical interactions (Fig. 16A). Batch incubation of the protein in Ni-NTA resin following by packing in the glass chromatography column was performed (Fig. 16B). The opaque-amber first fraction (wash buffer) containing residual proteins was set apart. Then, the second fraction was extracted by means of elution buffer which allowed the reddish-brown CAT2_D120A protein be drained. The high resolution purification process ended with a diafiltration in order to change the elution buffer (rich in Imidazole) to phosphate buffer (Na^+/K^+) at pH= 7.8 and then the brown-color fraction containing the metalloenzyme was storaged at 4°C.

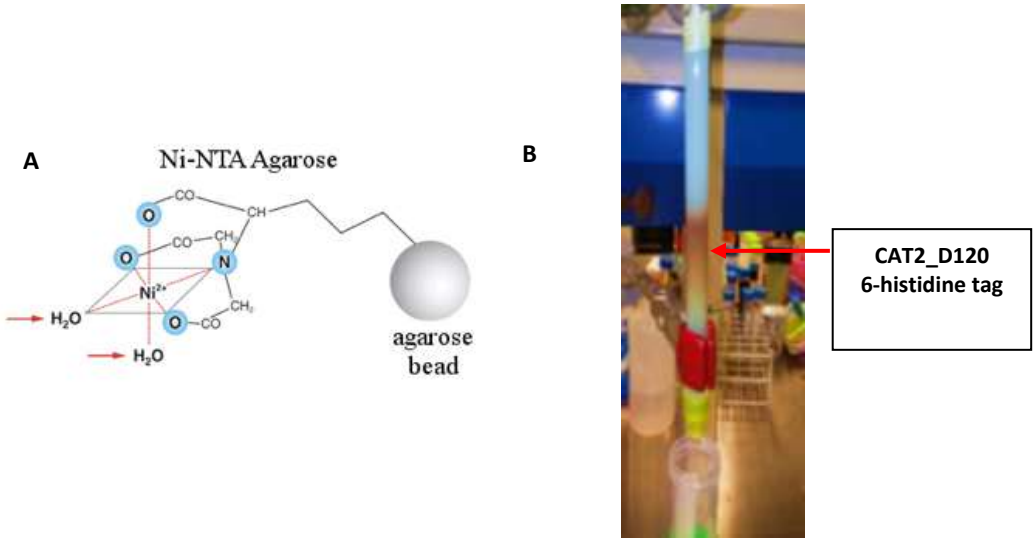

Fig. 16 A: Structure of Ni-NTA resin[40] with two labile positions to interact with histidine tagged proteins and B: CAT2_6H-D120A purification with Ni-NTA resin.

5.1.3 Quantification by Bradford method and determination of Reinheitszahl ratio (Rz).

The Bradford Coomassie brilliant assay was accomplished by measurement of absorbance at 595 nm and a BSA calibration curve (Fig. A1) were used to determine final concentration of the protein after purification process for CAT2_WT and its variant CAT2_D120A. The increment in absorbance (595 nm) when the protein was present in the solution is the expected experimental result. Initially, free dye was reddish brown color, when the dye interacts with the denaturing protein, it turned in blue color.[32] The main advantage of this method consist in researches can follow the absorption measured at 595 nm using a spectrophotometer, which is related to the proportion of dye bounded to the exposed amino acids of the protein of interest. Thus, concentrations of CAT2_WT and CAT2_D120A variant are presented in Table 1.

Table 1. Concentration of D120A determined by Bradford method and Reinheitszahl ratio (Rz).

CAT2_H6	**Concentration (mg/mL) $\lambda_{595\ nm}$**	**$R_Z = A_{soret}/A_{280}$**
WT	22,03	0,54
D120A	15,12	0,58

Reinheitszahl ratio[41], Rz, is calculated by the relation of absorbance between Soret band (≈400 nm) and amino acid aromatic absorption (≈280 nm) and makes an estimate about the amount of heme type-*b* incorporated after expression and purification. Rz value is important to the biochemical activity since the activity of the protein depends directly on the heme-*b* incorporated to the protein. Typical values of Rz for CAT2_WT have been reported in the range of 0.56-0.57[27], the obtained value for D120A variant is consistent with those values, thus indicating that the mutation in aspartate-120 do not affects the biosynthesis of heme incorporation.[42] For a homodimeric proteins like CAT2_WT and D120A, Rz values around 0,5 demonstrates the presence of only one heme-*b* per dimer.

5.1.4 Size characterization by denaturing electrophoresis SDS PAGE

The assay using SDS polyacrylamide gel (8%) in the electrophoresis technique allowed elucidates one predominant band at 84 kDa that corresponds to monomer and other faint band around 177 kDa which is recognized to homodimer of CAT2_D120A metalloenzyme (Fig 17).

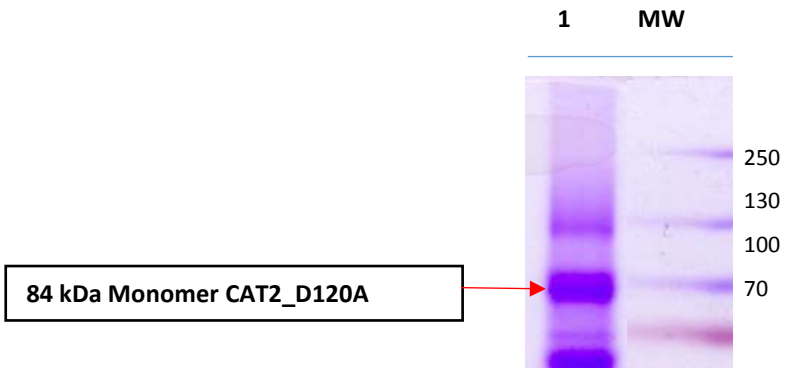

Fig. 17 SDS PAGE electrophoresis of CAT2_D120A revealed with comassie blue.

5.1.5 Zymography of peroxidase and catalase activity.

Native polyacrylamide gel (8%) with the protein loaded was subjected to electrophoretic process with non-reduction and non-denaturing agents. Zymograms were evaluated to determine peroxidase and catalase activity as described in methodology section. After the incubation in sodium acetate buffer, o-dianisidine and H_2O_2 bubbles and two yellow bands were observed in the peroxidase zymogram (Fig. 18A), confirming the presence of peroxidatic function for both subunits in CAT2_D120A.

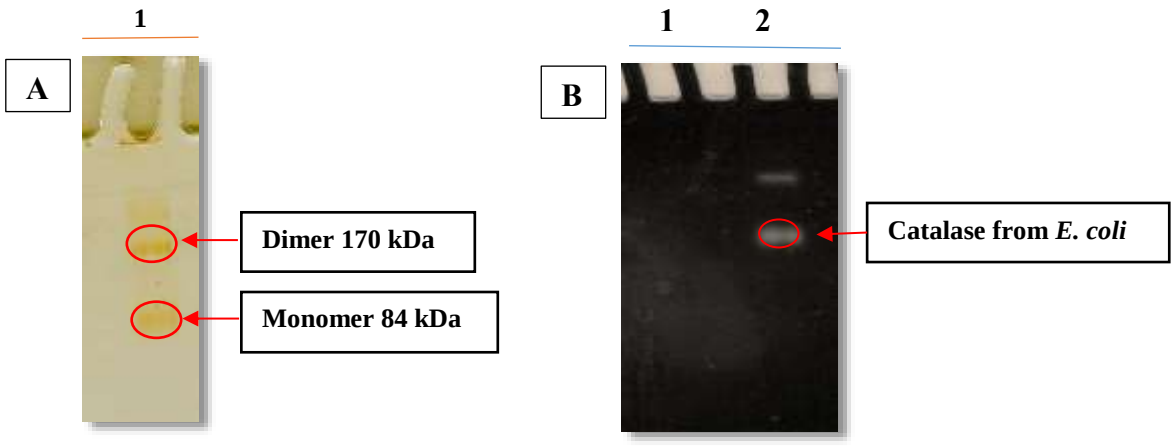

Fig. 18 Zymograms of **A**) Band:**1**: peroxidase activity for CAT2_6H-D120A and **B**) Catalase activity for . Bands:**1:** CAT2_6H D120A**, 2:** *Echerichia coli* catalase activity

On the other hand, catalase zymogram was performed loading 20µg of the D120A protein in *line 1* and 20µg of catalase from *E. coli* were loaded in the *line 2* in the polyacrylamide gel to make a comparison. Incubation of native gel in H_2O_2 solution during 5min followed by the oxidation reaction using $K_3[Fe(CN)_6]$ (2%) and after $FeCl_3$ (2%) revealed that the absence of catalitic activity for the variant. A comparison for the catalase activity between D120A and *E. coli* catalase reveals unambiguously the lack of catalytic activity in the variant (Fig. 18B).

The engineering of the active site of catalase-peroxidase enzymes described in section 8.1, indicate that distal amino acids like MYT organic cofactor and aspartate 120 plays critical role on the catalase activity.[26] Thus, punctual variation of Asp120 interrupt the reaction mechanism of peroxide disproportionation *via* catalytic pathway as we expected.

5.1.6 UV-Vis spectroscopy characterization of CAT2_WT and CAT2_D120A variant

The electronic spectrum for the variant CAT2_D120A (3µg/uL) was obtained using phosphates buffer (Na^+ / K^+, 50mM. pH=7.8) as blank. The analysis at first instance is about UV-Vis electronic spectra with respect to electronic transitions on the porphyrin core in heme-*b* at the active site of the protein. Macrocyclic porphyrin (Fig. A2), is an 18 π e^- aromatic system, main absorption in its electronic spectra is around 400 nm with large values of absorptivity molar coefficient and assigned to an intramolecular charge transfer (π→π) well known as Soret band. Position of Soret band is highly dependent on the substituents in

porphyrin ring and the oxidation and in the cases of presence of a metal center, its spin states make an important contribution. Extensive classification of porphyrin derivatives is made based on the substituents on the ring. Specifically, heme groups contains an iron metal center and different substituents on C3, C8 and C18 carbons and a conventional nomenclature is well known in the literature. In the case of catalase-peroxidase enzymes, heme-*b* is founded as the active site (Fig. A2). Depending on the heme type (*a*, *b*, *c*, *o*, etc.) additional peaks in the range of 450– 700 nm (α and β) are expected.[43]

UV-vis spectrum of D120A variant presents a Soret band in 408 and two wide bands extended from 510 to 680 nm. According with the literature, this spectroscopic characteristic corresponds to oxidized Fe^{III}-heme *b* group. Compared with CAT_WT Soret band at 406 nm, those for the variant enzyme is almost unappreciable (Fig. 19B). Another spectroscopic feature is the wavelength value for protein absorption which is close to the theoretical value (280 nm) for the variant at 281 nm and for the wild type at 279 nm. This effect of Soret band shifting has been previously seen in recombinant catalases-peroxidases of bacterial species[44] and other CAT2 variants (W90A and R426A)[32] from *N. crassa* fungus. Additionally, the substitutions on the aminoacidic sequence of those manifest the loss of catalase function but those keep the peroxidase activity which also was seen in the Zymography (Fig.18B) for our CAT2_D120A.

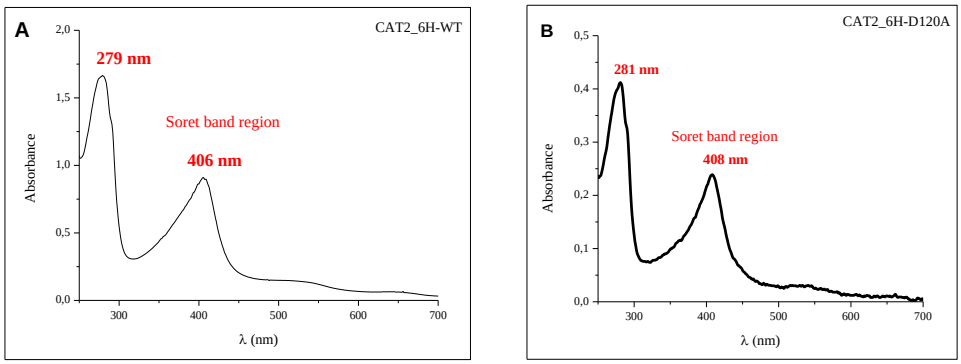

Fig. 19 UV-Vis spectra of A) CAT2_6H-WT and B) CAT2_6H-D120A with 3μg/μL of concentration.

5.1.7 Redox properties. Oxidation state of iron in CAT2_D120A

CAT2_D120A was isolated in oxidized form as we saw previously; a preference for ferric state instead of ferrous state in native form is observed. In order to demonstrate

unambiguously the oxidation state of iron in heme *b*, a chemical redox reduction with disodium dithionite was performed. Solved dithionite in water solution presents a dissociation in two molecules: $S_2O_4^{2-}$ and $2SO_2^{\bullet -}$ anionic radical, such anion has been confirmed as the reducing agent of Fe^{III}-heme in several proteins.[45] The chemical reactions are described below:

$$S_2O_4^{2-} \rightleftharpoons 2SO_2^{\bullet -}$$

$$SO_2^{\bullet -} + bHFe^{III} \longrightarrow bHFe^{II}$$

UV- Vis spectroscopy was used to follows the reduction of the CAT2_D120A, after mixing protein with an excess of sodium dithionite, a displacement of the Soret band from 408 nm to 421 nm is observed (Fig. 20). Such Soret red-shift displacement is the evidence of the reduction of iron in heme-*b* and is in agreement with previous reported works. For example, ferric cytochrome *c* protein from *E.coli* (apo-CcmE´) evidenced a shifting from 413nm to 425 nm (Fig. A3)in the Soret band for the reduction reaction.[46] The bathochromic shifting in Soret band and formation of Q-bands (541nm and 576 nm) were proofs of the ferrous pentacoordinated hemic catalytic center formed during the reduction of the Fe^{III}-oxyhemoglobin isolated from human red blood cells.[47]Additionally, CAT2_WT revealed a red shift from 401nm to 437 nm in the Soret band and the formation of the two characteristic peaks at 556 nm and 593 nm after reduction with dithionite.[27]

In our case, red-shifted displacement of Soret band is evident in Fig. 20, however, the expected peaks located at Q-band region could not be displayed in comparison to the values described for the CAT2_WT in Fig. A4 in the appendix due to the protein concentration was lower.

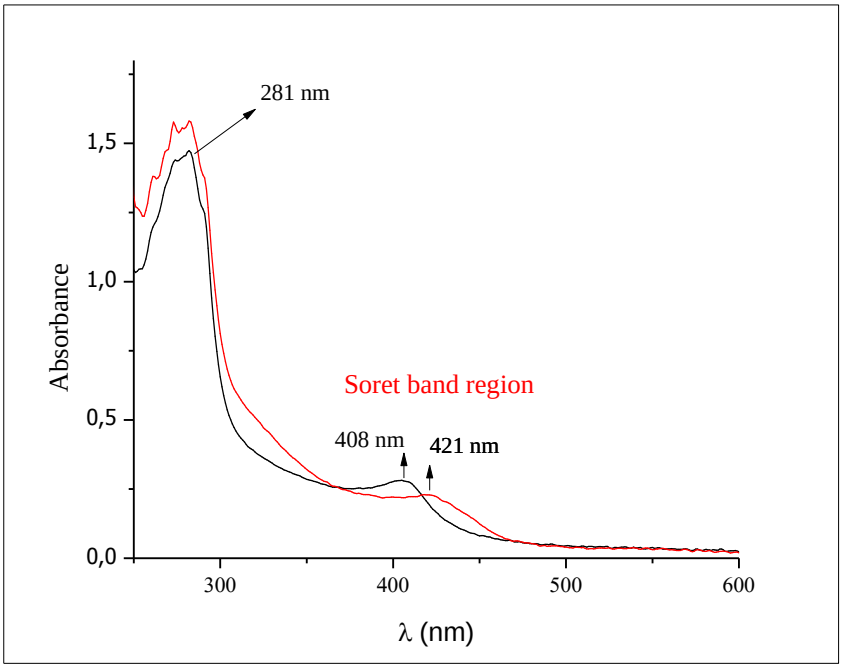

Fig. 20 Electronic spectra of the Fe^{III}-heme *b* in CAT2_D120A 3µg/µL as isolated (—) and after reduction with disodium dithionite (—).

5.1.8 Spin state determination of iron in CAT2_D120A.

UV-Vis spectroscopy. The previous results demonstrated that the variant presents a ferric oxidation state in the heme *b* of CAT2_D120A in its resting state. Now, spin state determination is essential to understand the electronic environment of iron in the active site. Thus, D120A (10^{-4}M) variant was incubated during 1 hour at 4 °C with 1000 fold excess of KCN. A bathochromic shifting of 17 nm of the Soret was observed in the UV-vis spectrum of the incubated mixture (Fig. 21). Such shift is explained based on the coordination of cyanide molecule to the ferric center. As we now from the literature, CN^- is a strong-field ligand (Fig. A6) capable to modify electronic environment on iron. Soret band modification when CN^- is coordinated is an evidence that ferric-heme *b* is in a High Spin state in the protein as isolated.

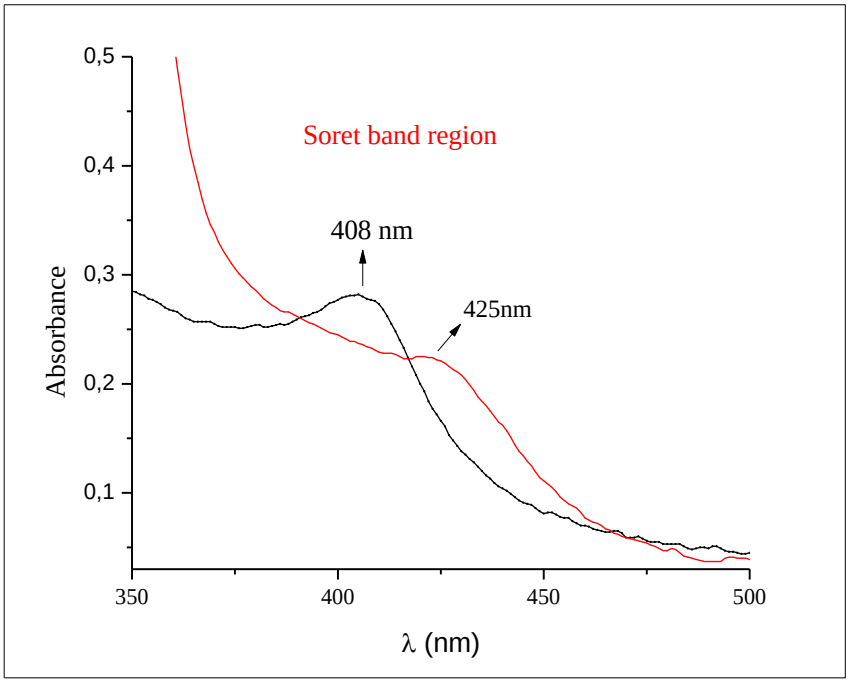

Fig. 21 High spin Fe^{3+} - hemic enzyme in phosphate buffer, pH= 7.8, at T= 22 °C (——). Low- spin Fe^{3+} hemic complex formation after the incubation of 200µL of the metalloprotein with KCN in phosphate buffer, pH=7.8, at T= 4°C ( ).

Comparatively, the shift in the Soret band for the CAT2_WT[27] from 401 nm to 418 nm in which cyanide ligand generated the same effect: the low spin Fe^{III}-heme formation. This is in agreement with our results for the variant. Another reports on the cyanide effect on iron electronic environment in which Soret absorbance values were displaced to red-region are those reported for KatG from *Synechocystis* PCC 6803 (406 nm to 422nm)[44]; WT- KatG (405nm to 423nm) and recombinant KatG[S315T] (405nm to 420nm) from the pathogen *Mycobacterium tuberculosis*.[36] Additionally, intracellular eukaryotic KatG from *Magnaphorte grisea phytopathogenic* fungus (MagKatG1) exhibited a shift from 408nm to 421nm.[48]These previously published experimental evidence suggest that the resting state for the CAT2_D120A is in a HS-Fe^{3+} state.

EPR spectroscopy. In order to complement the determination of iron spin state in D120A, EPR experiments to assign such spin sate were performed. The effectiveness of EPR technique to characterize biological and chemical paramagnetic substances in any aggregation state provided an advantage over other techniques. In the literature is reported that EPR of no entire spin sate species can be observed in X-band (≈ 9 GHz) as is the case of

Fe^{3+}.[12]Thus, an EPR experiment at low temperature (10 K) for CAT2_D120A was performed. The EPR spectrum taken at X-band (9, 386876 GHz, Fig 20) displayed an axial spectrum with characteristic signals around g = 6 and g = 2 values assigned to the hemic HS-Fe^{3+}. These results are in agreement with those reported for *b*-type heme in high spin state in metahemoglobin (Fig. A5 in the appendix).[49] Additionally, a mixture of signals in g = 6 region is observed in our case documenting the presence of at least two HS-Fe^{III} species contributing to the signal.[27,50] This mixture was observed and explained in terms of contribution of a combination of a more axial with g_x = 5.6895, g_y = 5.1794 and g_z = 2.001 and a more rhombic second component with g_x = 6.6235, g_y = 5.9000 and g_z = 2.001. Finally, peak with g = 4.2697 was attributed to the degraded heme out of axial and rhombic symmetries. Fig. 22.

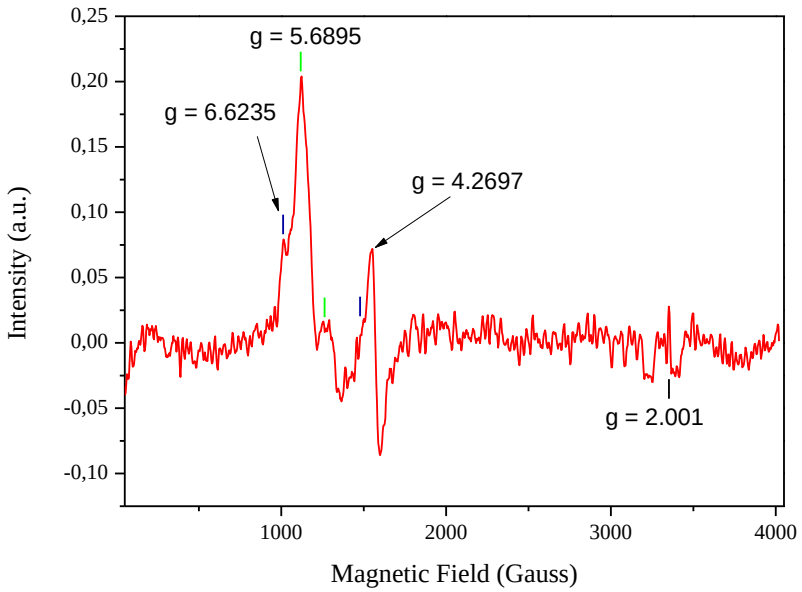

Fig. 22 EPR spectrum of CAT2_D120A as isolated at 10K.

Both, UV-vis and EPR results presented in this section are in concordance and gives evidence for the assignation of high spin state of iron in heme-*b* of D120A variant in resting state.

5.1.9 Study of intermediates of the catalytic reaction of CAT2_D120A

High valent oxo-iron compounds formed during the catalytic cycles of metalloenzymes have been object to study in order to understand the important dioxygen activation performed by nature. In the case of catalase-peroxidase enzymes, notable efforts to elucidate the reaction mechanisms of hydrogen peroxide cleavage have been made before. Specifically, in the case of CAT2 from Neurospora crassa, important advances on the characterization of relevant intermediates have been reported. Thus, due to the importance of the distal amino acids to the catalytic activity in catalase-peroxidases, extensive studies on the effect of the punctual mutation on aspartate 120 over the generation of key intermediates will be presented in this section.

First, in previous sections, we demonstrate that CAT2D120A loss the catalase function, but it holds the peroxidase activity. In consequence, hydrogen peroxide continue being its substrate, however, isolation of intermediates of the catalytic mechanism is hard because they are labile. Peroxyacetic acid (PAA) was used to help in the intermediates isolation.[44]

5.1.9.1 UV-Vis spectroscopy.

Formation of intermediates was performed by mixing the ferric enzyme as isolated (10^{-4} M) with peroxyacetic acid, the reaction progress was followed by UV-Vis spectroscopy. An interesting spectrum was obtained one minute after the beginning of the reaction in which a set of absorbance were obtained: 579nm, 583 nm and 594 nm in the Q-band region (Fig. 21 red line). If we compare those spectroscopic features with those of the CAT2_WT, an evident change is observed after the reaction with PAA. In the literature, similar changes for the products of the reaction of PAA with other catalase-peroxidases are assigned to the formation of an intermediate with a high valent oxo-iron in the presence of cationic porphyrin radical. Such intermediate is well known as Compound I (Fe^{IV}=O $Por^{\cdot+}$). For example, appearance of bands in Q-region in the range 540–650 nm for the same experiment but different catalases-peroxidases as KatG from *Synechocystis* PCC 6803 (640 nm & 643nm)[44]; KatG from *Mycobacterium tuberculosis* (MytKatG) incubated with PAA showed new Q-band values (550nm & 590nm)[50]; Bacterial b-type heme chlorite dismutase (Cld) reported

new absorbance values (585nm & 650nm)[51] and BpKatG mixed with 15-fold excess of PAA displayed the formation of two bands at 1 second see Fig. A7 (545nm & 585nm).[37]

Making a comparison of our spectral changes after the reaction with PAA with the values founded by the literature mentioned in the region 540-650 nm, allows us conclude that a Compound I intermediate was formed.

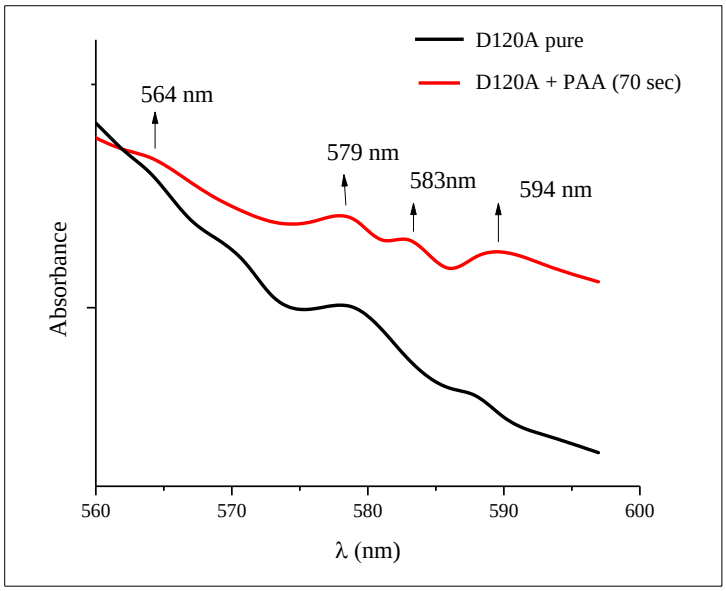

Fig. 22 Uv-vis spectra of CAT2_D120A as was isolated (—) and after 70 sec of reaction with peroxyacetic acid (—).

5.1.9.2 EPR spectroscopy.

Following the idea of the experiments presented in last section, a mixture of D120A variant with PAA was made, some aliquots of the mixture was taken and frozen in liquid nitrogen at different times. The sample taken 5 seconds after mixing presented a big change in its EPR spectrum compared with those obtained for the resting state. Disappearance of g = 6 documenting a change in the oxidation state of iron from Fe^{III} to Fe^{IV}; and the appearance of an intense signal in g = 2 region (Fig. 23), which accounts for the presence of a free radical species, allow us assign this spectra to a free radical centered in porphyrin cationic ring of a Compound I (Fe^{IV}=O Por$^{\cdot+}$). This is in a concordance with the result obtained by UV-Vis spectroscopy. Interestingly, no signal for paramagnetic Fe^{IV} is observed, this fact is explained considering that this Fe^{IV} is a d^4 HS species with an integer spin of S = 2 which is an EPR-

silent species because the Kramer´s doublets (Fig.A7). So for integer spin systems magnetic quantum number (m_s) are more separated between their pairs ($m_s = \pm ½$; $m_s = \pm 3/2$ and $m_s = \pm 5/2$) even at zero magnetic field and X-band radiation in EPR is not enough to generates the splitting of energy levels and in consequence the signals are weak.[12]

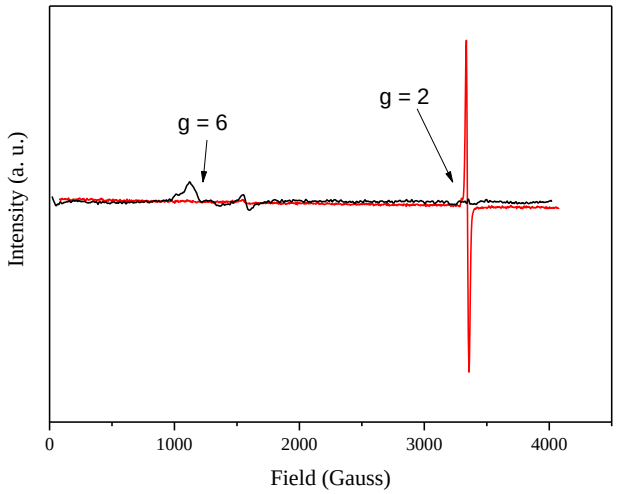

Fig. 23 EPR spectra of CAT2_D120A as isolated (—) and after 5 sec of reaction with peroxyacetic acid(—).

As in the case of the results for the high valent oxo-iron intermediates characterization, these results are strong evidence of the presence of an inner sphere electron transfer between iron and peroxide in the catalytic reaction cycle presented in Fig. 24 in blue.

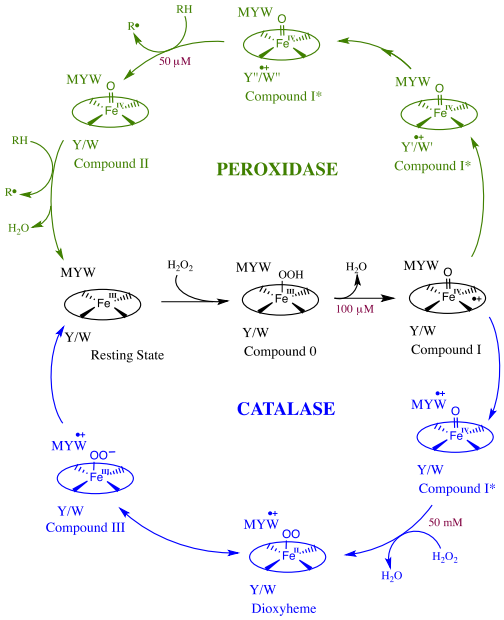

Fig. 24 Reaction mechanism of the bifunctional CAT2_WT from *N. crassa* fungus.

5.2 Results on the synthesis and characterization of a biomimetic model based on chlorophyll derived ligands coordinated to iron(II)

Approach on an initial proposal related to assemble a bioinorganic system able to mimic the structure of heme active site of an enzyme requires the extraction and refinement of starting ligand: Pheophytin (pheo) is a derivative from chlorophyll (Chl) pigment. In Fig.25. Chlorophyll and two derivatives are presented, the three structures varying in the R substituents at C-7 position.

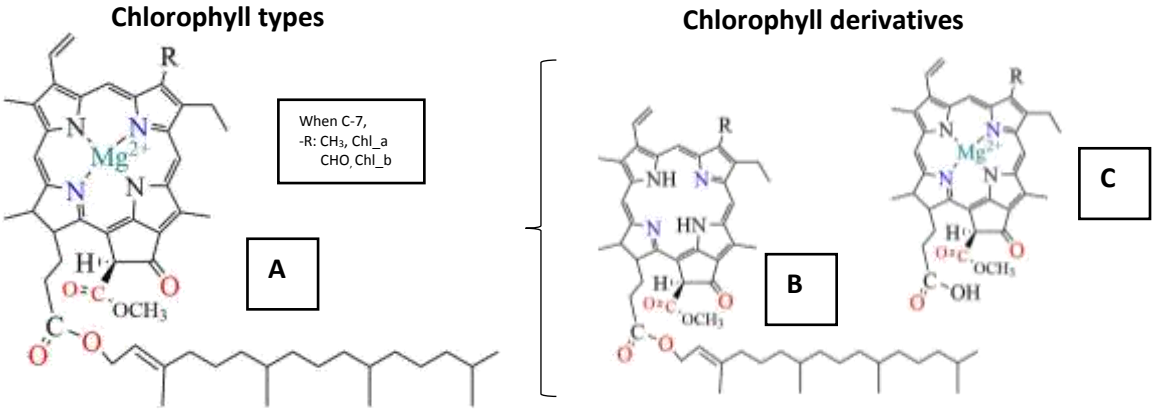

Fig. 25 Basic structure of Chlorophyll (A) and two derivatives, pheophytin (B) and chlorophyllide (C).

5.2.1 Isolation and characterization of Chlorophyll derivatives

5.2.1.1 Extraction of chlorophyll.

Spinach was mashed until its leaves lost the green color. Distilled water was poured and two phases were separated with a separating funnel and two phases were formed. Organic acetone-diethyl ether phase presented a dark-green color due to most of products were chlorophyll derivatives, however, xanthophyll and carotene are present in the extract and a further purification was needed.(Fig. 26)

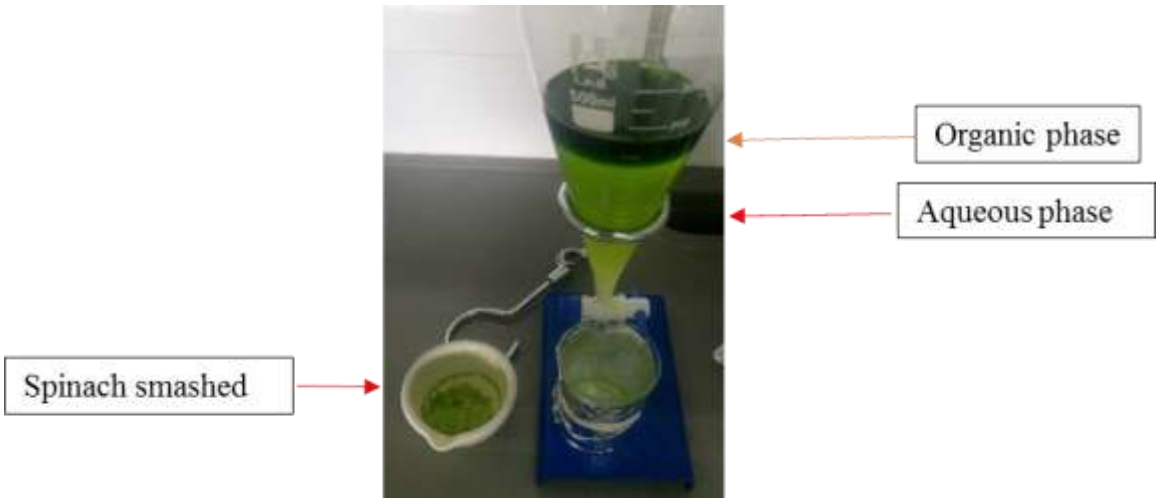

Fig. 26 Chlorophyll extraction from spinach by liquid-liquid extraction.

5.2.1.2 Thin Layer Chromatography (TLC).

Identification of the presence of chlorophylls (Chl) derivatives (Fig. 8), mixture of Chl_*a*, Chl_*b*, pheophytins, chlorophyllides and pheophorbides in the spinach extract, was achieved thin layer chromatography. TLC was run using a chromatographic chamber with mobile phase[39]: Hex 6: EE 3: Ac 2. Subsequently, silica-gel column was prepared to do purification process in order to separate de Chl derivatives from another pigments such as xanthophyll and β-carotenes as was described in section 4.1.

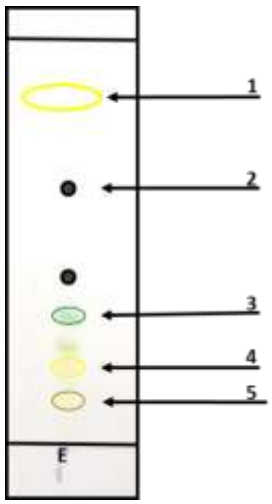

Fig. 27 TLC of Spinach crude extract. MP: Hex 6: EE 3: Ac 2.

TLC spots of crude extract could be reveled with a naked eye (Fig.27) due to the nature of the components; however, they were confirmed using UV-lamp. Rf results are recorded in the Table 1. Spot N° 1 is assigned to β-carotene; Spot N°2 with a Rf = 0.65 was assigned to pheo by comparison with the literature. Spot N° 3with Rf = 0.35 is defined as Chl_*b* because is closer to range reported in literature.[39] The same situation for orange spot N° 4 with Rf = 0,22, which is not in range reported but follows the pattern reported for Xanthophylls. At the end, gray-orange spot N° 5 that has Rf = 0,17 is registered as one oxidized chl-derivative known as pheophorbide_*b*. Each spot was classified according to literature reported with the mobile phase used in this work.

Table 1 Thin layer chromatography technique used to identify chl-derivatives and comparate with literature Rf-values.

Spot	**This work**		**Classification**	**From reference** [39]	
N°	**Spot color**	**Rf_value**		**Spot color**	**Rf_value**
1	Yellow	0.90	β-carotene	Yellow	0.9-1.00
2	Grey	0.65	pheo_ *a*	Grey	0.59-0.65
3	Yellowish green	0.35	Chl_*b*	Yellowish Green	0.39-0.45
4	Orange	0.22	Xanthophyll	Orange	0.25-0.28
5	Grey-orange	0.17	Pheophorbide *b*	black	0.17-0.20

A column chromatography was used in order to separate the Chl_b desired. From the column chromatography, thirty test tubes were drained but only three were candidates to be identified as chl - derivatives. This was performed after run several TLC plates in which 6 - 8 numbered fractions (Fig.28) of 7 ml were chosen and then homogenized in a dark vial stored at 4 °C to avoid oxidative process.

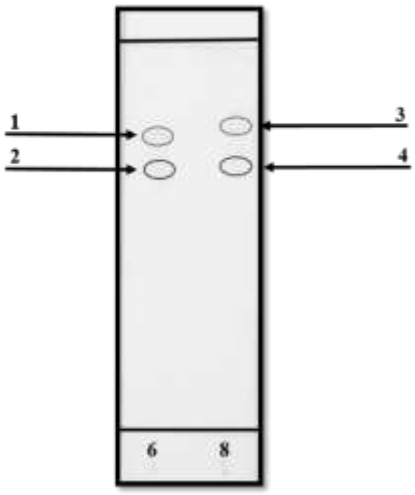

Fig. 28 TLC plate of test tubes 6-8 after of column-separation process. MP: Hex 6: EE 3: Ac 2

According to Fig. 28 we made the assignation showed in Table 2, thus spots N° 1 and N° 3 were visible using the mobile phase in the chamber, however under UV-light lamp two additional spots: N°2 and N°3 were revealed. In the case of N°1 which was grayish–green color with Rf = 0.7, it was associated to pheo_*a*. Spot N°2 is considered as mixture of pheo_a and pheo_b assigned by the reported color spot and Rf = 0.65 as well as the Spot N° 4. Finally, Spot N° 3 is considered a mixture between chlorophylls derivatives (the most abundant pigment) and a little bit of any carotene due to its Rf value.

Table 2 Thin layer chromatography technique used to classify test tubes in which were chl-derivatives using Rf values and qualitative characterization argued in literature.

Spot	**This work**		**Identification**	**From references**	
N°	**Spot color**	**Rf_value**		**Spot color**	**Rf_value**
1	Gray-green	0.7	pheo_ *a*	Gray [39]	0.59-0.65
2	Gray to Transparent	0.65	pheo_ *a & b*	Bluish-gray, reveled under UV-light [52]	0.59-0.65 [39]
3	Gray-green	0.8	Mix of Chl-derivatives and β-carotene	-	0.39-0.45
4	Gray to Transparent	0.67	pheo_*a & b*	Bluish-gray, reveled under UV-light [52]	0.59-0.65 [39]

5.2.1.3 UV-Vis characterization of Chl and its derivatives.

UV-Vis spectra of chlorophyll derivatives were taken using acetone: water (9:1) mixture as blank of the measurements. A Soret band displaying a maximum value at 431 nm and two peaks at 384.5 nm and 410 nm are present. Additionally, three peaks of minimum absorbance at 535 nm, 581 nm and 617nm, and a maximum at 663 nm in the Qy band region were observed (Fig. 29). According to literature, values are corresponding to chl_*a* pigment and that are mainly characteristic of porphyrin-like systems. We need to remember that porphyrin are aromatic system that follows the Hückel´s rule (4n+2) and in this case chlorophyll derivatives share a core denominate "chlorin" in which one outer double bond is hydrogenated (only 20 π-electron), but the π-delocalization on tetrapyrrole is not affected, and aromaticity is maintained producing the highlighted peaks in the spectrum.[43]

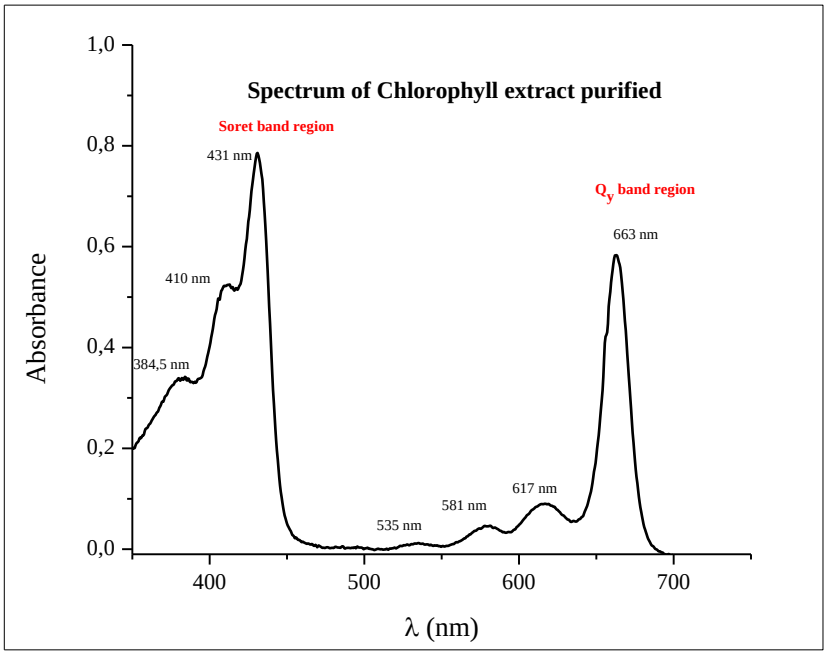

Fig. 29 UV-Vis spectrum of purified chlorophyll fraction.

Next step in our synthesis strategy involves the extraction of Mg^{2+} cation from chlorophyll, thus, by using HCl concentrated to obtain a demetallized structure, and the pheophytin (Fig. 25B). Isolated pheophytin presents a different UV-vis spectrum compared with the chlorophyll one. From this spectrum, stand out the Soret maximum value at 413 nm in comparison to chl-Soret band at 431 nm, displayed a shifting to higher energy region, but in the case of Q-band pheo at 667 nm and chl_*a* at 667 nm, it showed a shifting to lower

energy region. Additionally, five peaks appeared between soret and Q band that could be attributed to the presence of chlorophyllide (lost of phytil tail of hydrocarbon) as part of the mixture of chlorophyll degradation products (Fig. 30).

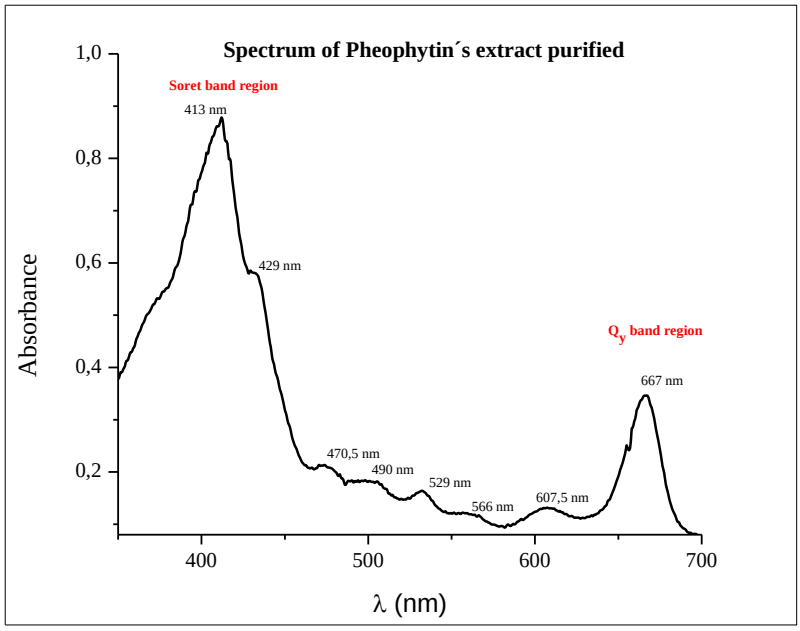

Fig. 30 UV-Vis spectrum of pheophytins obtained from the reaction of chlorophyll extract with HCl.

5.2.2 Synthesis of the Co^{2+} and Fe^{2+} complexes with pheophytin.

Qualitative chemical reaction between isolated pheophytins with Fe^{2+} and Co^{2+} salts separately were performed. Thus, Fe^{2+}-pheo complex exhibited a yellowish-green color, whereas Co^{2+}-pheo complex had turquoise color. The visualization of color change for both qualitative reactions in comparison to Chl pigment (dark green color) and pheo derivative (olive- green color)[53] gave us an idea of a successful coordination of metals. Another fact to be highlighted is the starting reagents were of colors totally different in contrast to the complexes formed (Fig.31).

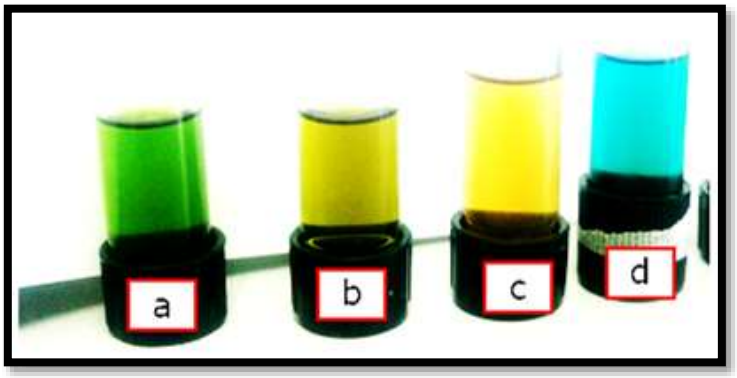

Reagent	Starting color
Pheo	
$[Fe(Cl)_2(H_2O)_4]$	
$[Co(H_2O)_6]Cl_2$	

Fig. 31 Qualitative demonstration of Metallic complexes chemical reaction. **a :** Chl**; b:** pheo**; c:** Fe^{2+} -pheo**; d:** Co^{2+}-pheo.

5.2.2.1 UV-Vis characterization of Fe-pheo complex

The yellowish-green **Fe^{2+}-pheo comple**x was characterized by UV-Vis spectroscopy, the obtained spectrum showing main shifting in Soret and Q bands in contrast to pheophytin and chlorophyll spectra. Spectra (Fig. 32) elucidated an important displacement of blue-band to shorter wavelength equals 393.5 nm when Fe^{2+} -pheo complex is formed in comparison to chl 431 nm and pheo 413 nm. Additionally, red-band in the case Fe^{2+} -pheo complex is broader and when value is compared to chl Q band at 663 nm and pheo Q-band 667 is clear the shifting to shorter wavelength.

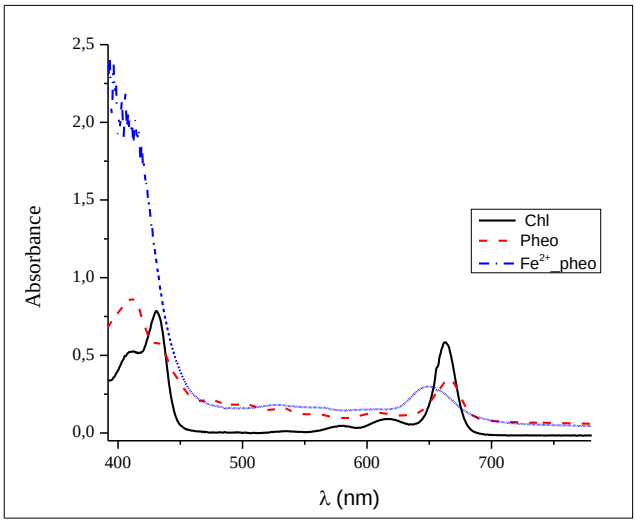

Fig. 32 Electronic absorption spectrum obtained for chlorophyll, pheophytin and Fe^{2+}-pheo.

Data experimental was reported using λmax that are in bibliography, Table N° 3 resume the values obtained by previous researchers in order to verify the coordination of Fe^{2+} atom into of pheophytin chlorin -nucleus. Thus, maximum value in soret-band region is really closer to value in literature 393.5 nm for Fe^{2+} -pheo complex, however value in Q-band region differs around 20 nm. This result could be attributed to pheo_*a* & *b* mixture despite of the bands for pheo_*b* cannot be identified as easily as those of pheo_ *a*, the bands of pheo_*b* could be masked by the broad bands of type *a*.

Table 3 Resume of electronic absorption experimental data obtained for chlorophyll, pheophytin and Fe^{2+}-pheo in contrast of literature reports.

	λmax (this work)		**λmax [38](from reference)**	
	Soret Band	**Q band**	**Soret Band**	**Q band**
Chl_*a*	431	663	432	664
pheo_*a*	413	667	409	665
Fe^{2+}-pheo	393.5	647	393	626

Co^{2+}-pheo complex characterization was made in order to make a comparison with the spectroscopic features of the Fe^{2+} -pheo complex. Thus, Co^{2+} -pheo complex[54] in Soret band region presented a shifting compared with spectrum of pheo_*a* from 413 nm to 418 nm. Also, in Q-band region complex formation generate a displacement from 667 nm to 687.5 nm in comparison to Q-band of pheo_a. Also, four peaks with minima absorbance between Soret and Q bands disappear when the metallic atom is coordinated and two news peaks one at 390 nm and 594 nm are remarkable in the spectrum of Co^{2+} -pheo complex suggesting the presence of free Co^{2+} (d^7-specie) in solution (Fig. 33).

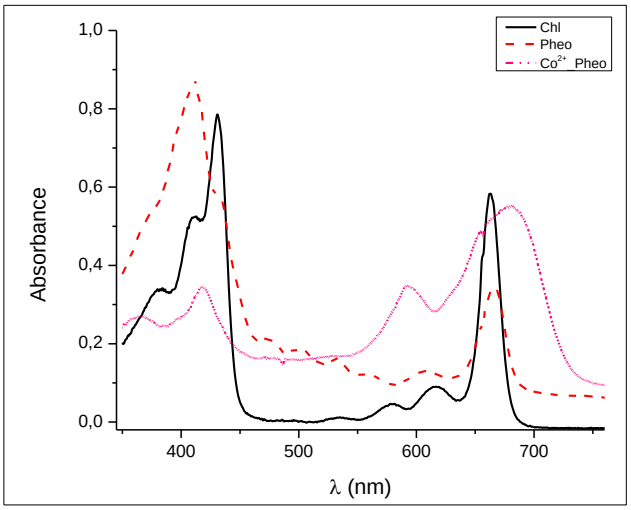

Fig. 33 Electronic absorption spectrum obtained for chlorophyll, pheophytin and Co^{2+}-pheo.

5.2.3 Evaluation of reactivity of Fe^{2+}-pheo against peroxyacetic acid (PAA)

In this section, results on the reactivity between Fe^{2+}-pheo against peroxyacetic acid (PAA) were performed with the objective of isolate synthetic oxo-iron intermediates following the conditions showed in next figure.

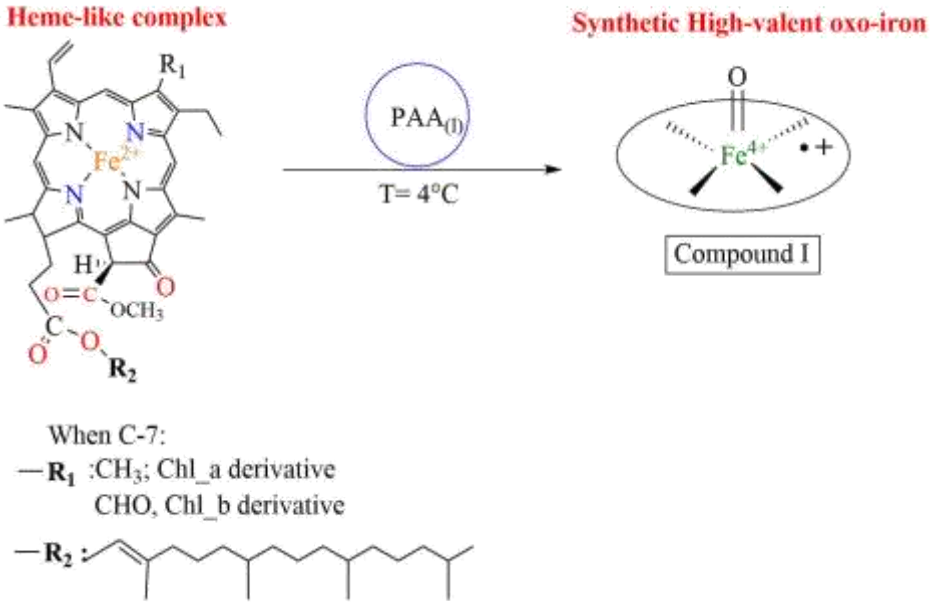

Fig. 34 Strategy of synthesis for the generation of oxo-iron species.

5.2.3.1 Kinetics of PAA reduction by Fe^{2+}-pheo followed by UV-Vis spectroscopy

Reactivity Fe^{2+}-pheo against peroxyacetic acid (PAA) was followed by UV-Vis spectroscopy. The progress of the reaction was followed by measurements of disappearance of the band centered in 395.5 nm characteristic of the Fe^{2+}-pheo complex. UV-Vis specra were recorded in 0.1 sec intervals during 10 seconds. Notable changes in the absorbance (395.5 nm) taken place until 3 seconds after te mixing of the reactants. Temperature was controlled at T=4°C with a peltier system. After that in the range of 1.5-2.8 secs, Soret-band (395.5 nm) almost disappeared which allows conclude the PAA was consumed completely and hence Fe^{2+}-pheo complex is capable to reduce peroxyacetic acid. (Fig. 35)

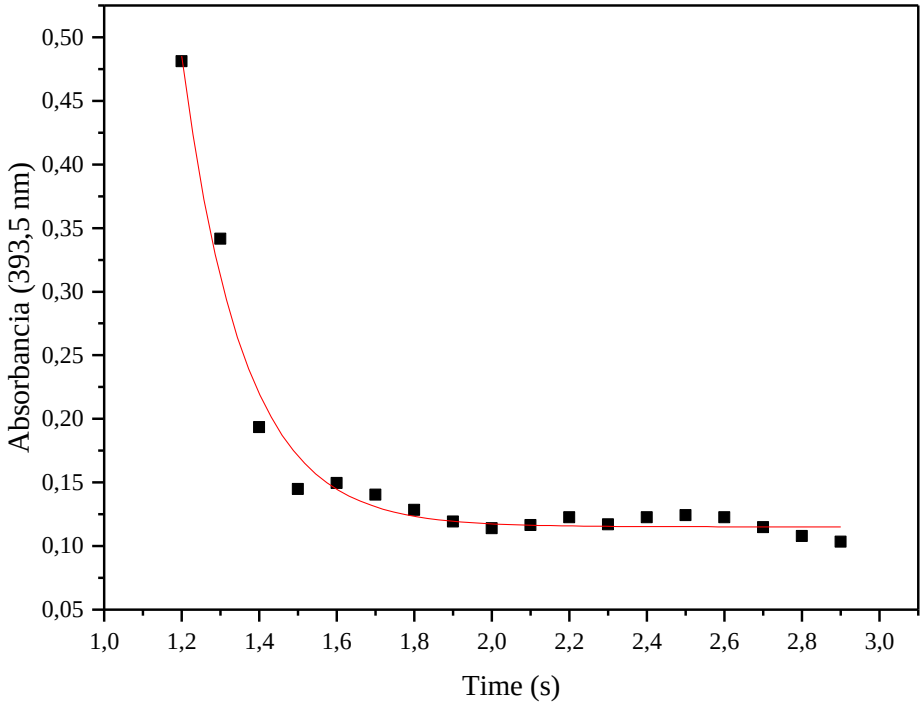

Fig 35. Kinetic of the reaction of Fe^{2+}-pheo complex with PAA.

5.2.3.2 EPR characterization of the product of the reaction between Fe^{2+}-pheo and PAA

In order to determine the nature of the compound obtained from the last reaction, EPR characterization was made. An aliquot of the reaction mixture was taken after 10 seconds of the beginning of the reaction. EPR spectrum shows a broad signal centered in g = 2.0308

which can be assigned to and Fe^{3+} LS (Fig. 36). Similar EPR results were reported for some inorganic complexes with iron (III) LS.[55]

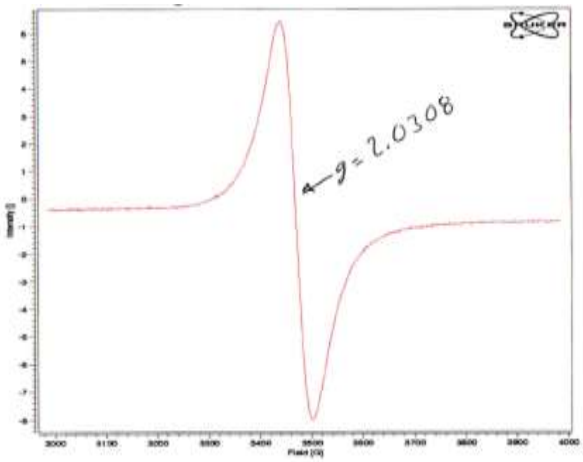

Fig 36. X-band EPR spectrum at 100 K of the mixture of Fe^{2+}-pheo complex with PAA at 7 sec of reaction.

From the kinetic results, is evident that iron compound can do the homework of the peroxide activation, additionally a change in the oxidation state of iron is documented by the comparisson of the EPR spectra for de diamagnetic Fe^{2+}-pheo in which a d^6 species don't show EPR signal (Fig. A8) with these obtained after the reaction with PAA (Fig. 36). Unfortunately, no evidence of oxo-iron (Fe^{IV}=O) species was reveal in such experiments, however, further work on the modification of the pheophytin ligand could be performed in the near future.

6. Summary & Conclusion

CAT2_D120A histidine-tagged enzyme variant was constructed by molecular biology techniques and purified by chemical affinity chromatography with a Ni-NTA resin in high yields. Rz value of 0.57 for the enzyme determined by UV-Vis indicates that D120A incorporates heme group at the same level of the Wild Type. Zymmogram experiments showed that the enzyme preserves their peroxidatic activity but loses their catalytic activity; later result is in concordance with punctual mutation located in the distal part of the active site of the enzyme, which is responsible for the catalase activity. EPR results demonstrated the presence of a group of signals in the regions of g = 2 and g = 6 assigned to an iron (III) in High Spin state, additionally, Fe(III) oxidation state was confirmed by UV-Vis spectroscopy. Similar spectroscopic properties were observed for the WT_CAT2 indicating that iron remains intact in the active site of the mutant. Finally, with the reaction of the variant with PAA it was possible to artificially generate a ferryl intermediate which was characterized by UV-Vis and EPR spectroscopies, in particular EPR spectrum demonstrate (g = 2.003) the presence of a free radical in a compound that is assigned to the species known as Compound I (Fe^{IV}=O Por+•). Thus, we fulfill with the one of main objective ok this work: "The isolation and characterization of a biologic oxo-iron intermediate".

The progress of an inorganic complex inspired in the heme-*b* active site from CAT2 was achieved, Fe^{2+}-pheo, which was synthetized from chlorophyll derivatives and adequately characterized. Thus, UV-Vis spectroscopy showed the maxima values of absorbance for Fe^{2+}-pheo in the Soret band (393.5 nm) and Q-band (647 nm). Meanwhile, the reactivity evaluation of the complex in front of a chemical reaction with PAA resulted in a consumption by part of Fe^{2+}-pheo showing a decreasing in the Soret band. Finally, the EPR spectrum reveled a characteristic peak of $LSFe^{3+}$ specie during the chemical reaction between Fe^{2+}-pheo and PAA, that indicated the generation of an oxidized form of our inorganic complex.

Although, we did not see the formation of a high valent oxo-iron in the evaluation of reactivity for the Fe^{2+}-pheo, it will continue being a motivation for studying, developing and improving of the inorganic system in search of Fe^{IV} and Fe^{V} species.

(1) Dauphas, N.; Rouxel, O. Mass Spectrometry and Natural Variations of Iron Isotopes. *Wiley Intersci.* **2006**, 515–550. https://doi.org/10.1002/mas.20078.

(2) Meija, J.; Coplen, T. B.; Berglund, M.; Brand, W. A.; De Bièvre, P.; Gröning, M.; Holden, N. E.; Irrgeher, J.; Loss, R. D.; Walczyk, T.; et al. Atomic Weights of the Elements 2013 (IUPAC Technical Report). *IUPAC & De Gruyter* **2016**, *88* (3), 265–291. https://doi.org/10.1515/pac-2015-0305.

(3) Slukla, AK; Hariprakash, B. Iron. In *Encyclopedia of Electrochemical Power Sources*; Elsevier B.V.: Amsterdam, 2009; pp 744–745.

(4) Gaucheron, F. Iron Fortification in Dairy Industry. *Trends Food Sci. Technol.* **2000**, *11* (2000), 403–409.

(5) Barreto-Rodrigues, M.; Silva, F. T.; Paiva, T. C. . Optimization of Brazilian TNT Industry Wastewater Treatment Using Combined Zero-Valent Iron and Fenton Processes. *J. Hazard. Mater.* **2009**, *168*, 1065–1069. https://doi.org/10.1016/j.jhazmat.2009.02.172.

(6) Multani, R. S.; Feldmann, T.; Demopoulos, G. P. Antimony in the Metallurgical Industry: A Review of Its Chemistry and Environmental Stabilization Options. *Hydrometallurgy* **2016**. https://doi.org/10.1016/j.hydromet.2016.06.014.

(7) Saucedo Vázquez, J. P. Reacciones de Deshidrogenación Oxidativa Promovidas Por Hierro y Rutenio. Un Estudio Mecanístico., Universidad Nacional Autónoma de México, 2012.

(8) Schweitzer, C.; Schmidt, R. Physical Mechanisms of Generation and Deactivation of Singlet Oxygen. *Chem. Rev.* **2003**, *2*, 1685–1757.

(9) Huheey, James E; Keiter, Ellen; Keiter, R. *Inorganic Chemistry - Principles of Structure and Reactivity*, 4th ed.; HarperCollins Publishers, 1993.

(10) Atkins, Peter; Overton, Tina; Rourke, Jonathan; Weller, Mark; Armstrong, Fraser; Hagerman, M. *Inorganic Chemistry*, Oxford Uni.; Oxford University Press: Great

Britain, 2010.

(11) Apel, K.; Hirt, H. REACTIVE OXYGEN S PECIES : Metabolism , Oxidative Stress , and Signal Transduction. *Annu. Rev. Plant Biol.* **2004**, *55*, 373–399. https://doi.org/10.1146/annurev.arplant.55.031903.141701.

(12) Drago, R. S. *Physical Methods for Chemists*, 2nd ed.; Gainesviller, FL, 1992.

(13) Kenkel, I.; Franke, A.; Du, M.; Zahl, A.; Du, C.; Langer, J.; Filipovic, M. R.; Yu, M.; Puchta, R.; Fiedler, S. R.; et al. Switching between Inner- and Outer-Sphere PCET Mechanisms of Small-Molecule Activation: Superoxide Dismutation and Oxygen/ Superoxide Reduction Reactivity Deriving from the Same Manganese Complex. *J. Am. Chem. Soc.* **2017**, *139*, 1472–1484. https://doi.org/10.1021/jacs.6b08394.

(14) Comba, P.; Maurer, M.; Vadivelu, P. Oxidation of Cyclohexane by High-Valent Iron Bispidine Complexes : Tetradentate versus Pentadentate Ligands. *Inorg. Chem.* **2009**, *48* (24), 10389–10396. https://doi.org/10.1021/ic901702s.

(15) Ohlendorf, Douglas; Orville, Allen M; Lipscomb, J. D. Structure of Protocatechuate 3,4-Dioxygenase from Pseudomonas Aeruginosa at 2,15 A Resolution. *J. Mol. Biol.* **1994**, *244*, 586–608. https://doi.org/10.1006/jmbi.1994.1754.

(16) Denisov, I. G.; Makris, T. M.; Sligar, S. G.; Schlichting, I. Structure and Chemistry of Cytochrome P450. *Chem. Rev.* **2005**, *105*, 2253–2277.

(17) Zhang, R.; Newcomb, M.; Chandrasena, R. E. P.; Halgrimson, J. A.; Horner, J. H.; Makris, T. M.; Sligar, S. G. Cytochrome P450 Compound I. *J. Am. Chem. Soc.* **2006**, *128*, 4580–4581. https://doi.org/10.1021/ja060048y.

(18) Groves, J. T. Cytochrome P450 Enzymes: Understanding the Biochemical Hieroglyphs. *F1000Research* **2015**, *4* (May), 178. https://doi.org/10.12688/f1000research.6314.1.

(19) Stubbe, J.; Nocera, D. G.; Yee, C. S.; Chang, M. C. Y. Radical Initiation in the Class I Ribonucleotide Reductase : Long-Range Proton-Coupled Electron Transfer ? *Chem. Rev.* **2003**, *103*, 2167–2201.

(20) Klinman, J. P. How Do Enzymes Activate Oxygen without Inactivating Themselves ? *Acc. Chem. Res.* **2007**, *40*, 325–333. https://doi.org/10.1021/ar6000507 CCC:

(21) Draksharapu, Apparao; Rasheed, Waqas;Klein, Johannes E. M. N.;Que, L. Facile and Reversible Formation of Fe(III)-O-Ce(IV) Adducts from Nonheme Oxoiron(IV) Complexes and Ce(III). *Angew. Chemie - Int. Ed.* **2017**, *129* (31), 9219–9223. https://doi.org/10.1002/anie.201704322.

(22) Rohde, J. U.; In, J. H.; Lim, M. H.; Brennessel, W. W.; Bukowski, M. R.; Stubna, A.; Münck, E.; Nam, W.; Que, L. Crystallographic and Spectroscopic Characterization of a Nonheme Fe(IV)=O Complex. *Science (80-.).* **2003**, *299* (5609), 1037–1039. https://doi.org/10.1126/science.299.5609.1037.

(23) Costas, M.; Mehn, M. P.; Jensen, M. P.; Que, L. Dioxygen Activation at Mononuclear Nonheme Iron Active Sites : Enzymes , Models , and Intermediates. *Chem. Rev.* **2004**, *104* (612), 939–986.

(24) Bhakta, S.; Nayek, A.; Roy, B.; Dey, A. Induction of Enzyme-like Peroxidase Activity in an Iron Porphyrin Complex Using Second Sphere Interactions. *Inorg. Chem.* **2019**, *58* (5), 2954–2964. https://doi.org/10.1021/acs.inorgchem.8b02707.

(25) Vega Garcia, V. Sobre-Expresión de La Catalasa-Peroxidasa de Neurospora Crassa, Universidad Nacional Autónoma de México, 2007.

(26) Njuma, O. J.; Ndontsa, E. N.; Goodwin, D. C. Catalase in Peroxidase Clothing: Interdependent Cooperation of Two Cofactors in the Catalytic Versatility of KatG. *Arch. Biochem. Biophys.* **2014**, *544*, 27–39. https://doi.org/10.1016/j.abb.2013.11.007.

(27) Vega García, V.; Díaz-Vilchis, A.; Saucedo Vázquez, J. P.; Solano Peralta, A.; Rudiño Piñera, E.; Hansberg, W. Structure, Kinetics, Molecular and Redox Properties of a Cytosolic and Developmentally Regulated Fungal Catalase-Peroxidase. *Arch. Biochem. Biophys.* **2018**, *640*, 17–26. https://doi.org/10.1016/j.abb.2017.12.021.

(28) Solano-peralta, A.; Sosa-torres, M. E. Aplicación de Un Modelo Para La Interpretación de Espectros de Resonancia Paramagnética Electrónica de Sistemas Octaédricos de Cr (III). **2000**, No. October 2015.

(29) Palmer, G. Palmer, Graham. In *Special Assays and Techniques*; 1962; Vol. 9, pp 594–609.

(30) Tang, J.; Smulders, S.; Bousseksou, A.; Teat, S. J.; Li, Y.; Albada, G. A. Van; Gamez, P.; Reedijk, J. Two-Step Spin-Transition Iron (III) Compound with a Wide [High Spin-Low Spin] Plateau. *Inorg. Chem.* **2009**, *48* (5), 2128–2135.

(31) Shongwe, M. S.; Al-Rabii, S. H.; Al-Azani, M.; Muharbi, A.; Al-mjeni, F.; Matoga, D.; Gismelseed, A.; Al-omari, I. A.; Yousif, A.; Adams, H.; et al. Coordination Versatility of Tridentate Pyridyl Aroylhydrazones towards Iron : Tracking down the Elusive Aroylhydrazono-Based Ferric Spin-Crossover Molecular Materials. *Dalt. Trans.* **2012**, *41*, 2500–2514. https://doi.org/10.1039/c1dt11407g.

(32) Vega Garcia, V. En Busca de La Función de La Catalasa-Peroxidasa de Neurospora Crassa, Universidad Nacional Autónoma de México, 2011.

(33) Lledías, F.; Rangel, P.; Hansberg, W. Oxidation of Catalase by Singlet Oxygen. *J. Biol. Chem.* **1998**, *273* (17), 10630–10637. https://doi.org/10.1074/jbc.273.17.10630.

(34) Gregory, E. M.; Fridovich, I. Visualization of Catalase on Acrylamide Gels. *Anal. Biochem.* **1974**, *58* (1), 57–62. https://doi.org/10.1016/0003-2697(74)90440-0.

(35) Dutton, P. L. Redox Potentiometry: Determination of Midpoint Potentials of Oxidation-Reduction Components of Biological Electron-Transfer System. In *Methods in Enzymology*; 1978; Vol. LIV.

(36) Ranguelova, K.; Suarez, J.; Metlitsky, L.; Yu, S.; Brejt, S. Z.; Brejt, S. Z.; Zhao, L.; Schelvis, J. P. M.; Magliozzo, R. S. Impact of Distal Side Water and Residue 315 on Ligand Binding to Ferric Mycobacterium Tuberculosis Catalase - Peroxidase (KatG). *Biochemistry* **2008**, *47* (47), 12583–12592. https://doi.org/10.1021/bi801511u.

(37) Ivancich, A.; Donald, L. J.; Villanueva, J.; Wiseman, B.; Fita, I.; Loewen, P. C. Spectroscopic and Kinetic Investigation of the Reactions of Peroxyacetic Acid with

Burkholderia Pseudomallei Catalase-Peroxidase, KatG. *Biochemistry* **2013**, *52* (41), 7271–7282. https://doi.org/10.1021/bi400963j.

(38) Nelson, R.E; Ferruzzi, M. G. Synthesis and Bioaccessibility of Fe-Pheophytin Derivatives from Crude Spinach Extract. *J. Food Sci.* **2008**, *73* (5), 86–91. https://doi.org/10.1111/j.1750-3841.2008.00783.x.

(39) Kusmita, L.; Puspitaningrum, I.; Limantara, L. Identification , Isolation and Antioxidant Activity of Pheophytin from Green Tea (Camellia Sinensis (L .) Kuntze). *Procedia Chem.* **2015**, *14*, 232–238. https://doi.org/10.1016/j.proche.2015.03.033.

(40) Ritchie, C. Protein Purification. *MATER METHODS* **2012**, *2*, 134. https://doi.org///dx.doi.org/10.13070/mm.en.2.134.

(41) Shannon, Leland M.; Kay, Ernest;Lew, J. Y. Peroxidase Isozymes from Horseradish Roots. *J. Biol. Chem.* **1966**, *241* (9), 2166–2172.

(42) Carpena, X.; Loprasert, S.; Mongkolsuk, S.; Switala, J.; Loewen, P. C.; Fita, I. Catalase-Peroxidase KatG of Burkholderia Pseudomallei at 1.7 Å Resolution. *J. Mol. Biol.* **2003**, *327* (2), 475–489. https://doi.org/10.1016/S0022-2836(03)00122-0.

(43) Wijesekera, T. P.; Dolphin, D. Some Preparations and Preparations of Phorphyrins. **1985**, 229–266.

(44) Jakopitsch, C.; Rüker, F.; Regelsberger, G.; Dockal, M.; Peschek, G. A.; Obinger, C. Catalase-Peroxidase from the Cyanobacterium Synechocystis PCC 6803: Cloning, Overexpression in Escherichia Coli, and Kinetic Characterization. *Biol. Chem.* **1999**, *380* (9), 1087–1096. https://doi.org/10.1515/BC.1999.135.

(45) Cox, R. P.; Hollaway, M. R. The Reduction by Dithionite of Fe(III) Myoglobin Derivatives with Different Ligands Attached to the Iron Atom. *Eur. J. Biochem.* **1977**, *74* (3), 575–587. https://doi.org/10.1111/j.1432-1033.1977.tb11427.x.

(46) Daltrop, O.; Stevens, J. M.; Higham, C. W.; Ferguson, S. J. The CcmE Protein of the C-Type Cytochrome Biogenesis System: Unusual in Vitro Heme Incorporation into Apo-CcmE and Transfer from Holo-CcmE to Apocytochrome. *Proc. Natl. Acad. Sci.*

2002, *99* (15), 9703–9708. https://doi.org/10.1073/pnas.152120699.

(47) Dayer, M.; Moosavi-Movahedi, A.; Dayer, M. Band Assignment in Hemoglobin Porphyrin Ring Spectrum: Using Four-Orbital Model of Gouterman. *Protein Pept. Lett.* **2010**, *17* (4), 473–479. https://doi.org/10.2174/092986610790963645.

(48) Zamocky, M.; Uller, P. G. F.; Bellei, M.; Battistuzzi, G.; Stadlmann, J.; Vlasits, J.; Obinger, C. Intracellular Catalase / Peroxidase from the Phytopathogenic Rice Blast Fungus Magnaporthe Grisea : Expression Analysis and Biochemical Characterization of the Recombinant Protein. **2009**, *451*, 443–451. https://doi.org/10.1042/BJ20081478.

(49) Taiwo, F. A.; Le, L. Electron Paramagnetic Resonance Spectroscopic Studies of Iron and Copper Proteins. **2003**, *17*, 53–63.

(50) Svistunenko, D. A.; Worrall, J. A. R.; Chugh, S. B.; Haigh, S. C.; Ghiladi, R. A.; Nicholls, P. Biochimie Ferric Haem Forms of Mycobacterium Tuberculosis Catalase-Peroxidase Probed by EPR Spectroscopy : Their Stability and Interplay with PH. *Biochimie* **2012**, *94* (6), 1274–1280. https://doi.org/10.1016/j.biochi.2012.02.021.

(51) Lee, A. Q.; Streit, B. R.; Zdilla, M. J.; Abu-omar, M. M.; Dubois, J. L. Mechanism of and Exquisite Selectivity for O – O Bond Formation by the Heme-Dependent Chlorite Dismutase. **2008**.

(52) Thompson, Robert Bruce; Thompson Fritchman, B. *Illustrated Guide to Home Biology Experiments: All Lab, No Lecture*, 1st ed.; Jepson, B., Ed.; Dale Dougherty, 2012.

(53) Singh, A. Chlorophyll practice https://au-mynotebook.labarchives.com/share/Ashwin Singh/MjAuOHwyMjQ3LzE2L1RyZWVOb2RlLzExMDEwNDIyNDd8NTIuOA== .

(54) Dikio, E. D.; Isabirye, D. A. Synthesis and Oxidation of Cobalt (II) Pheophytin- a Complex. *E-Journal Chem.* **2011**, *8*, S297–S303.

(55) Astashkin, A. V; Raitsimring, A. M.; Kennedy, A. R.; Shokhireva, T. K.; Walker, F. A. Pulsed EPR Characterization of the Low-Spin Iron (III) Porphyrinate Complexes with Phenyl Isocyanide Ligands Having the d Xy Orbital Ground State. *J. Phyrsical Chem.* **2002**, *106*, 74–82.

Fig. A1 Calibration curve Bradford + BSA**.**

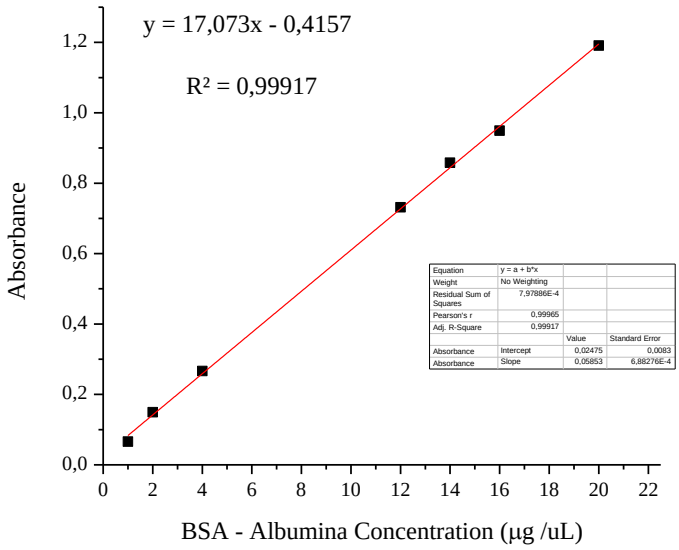

Fig. A2 Chemical structure of heme *b*

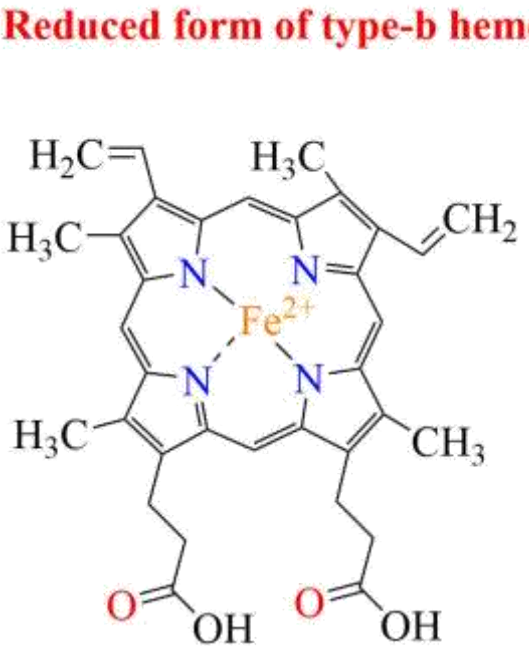

Fig. A3 UV-Vis spectra for reduced (·····) reacting with dithionite and oxidize (——) heme-b Cyt. The treatment with potassium cyanide (----). Taken from Daltrop.[46]

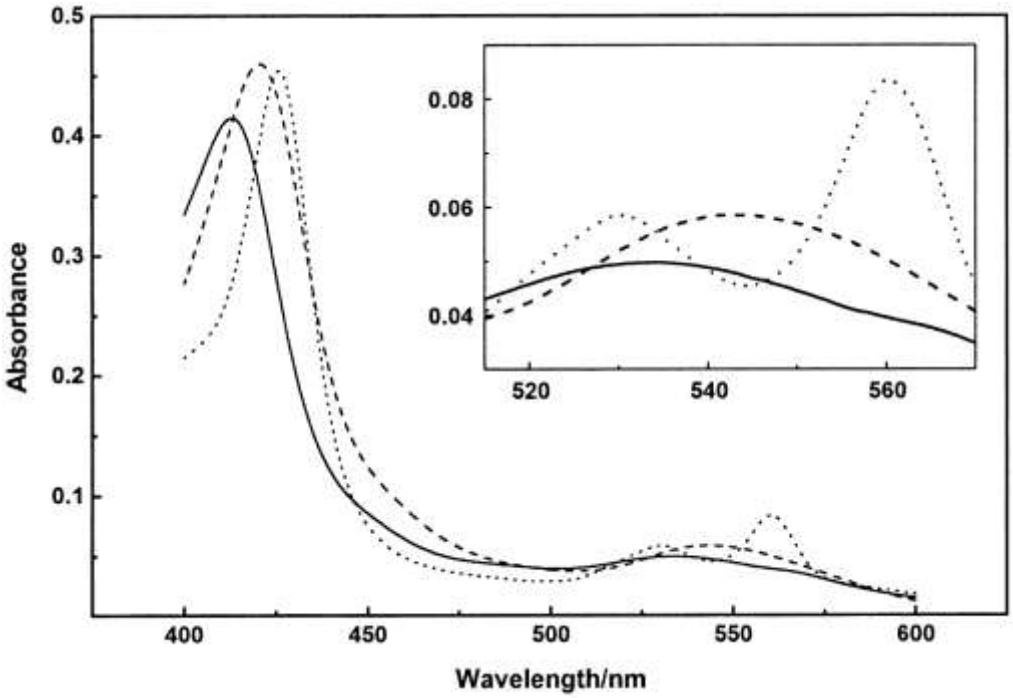

Fig. A4 UV-Vis spectra for CAT2_WT subjected to reduction reaction with sodium dithionite. [26]

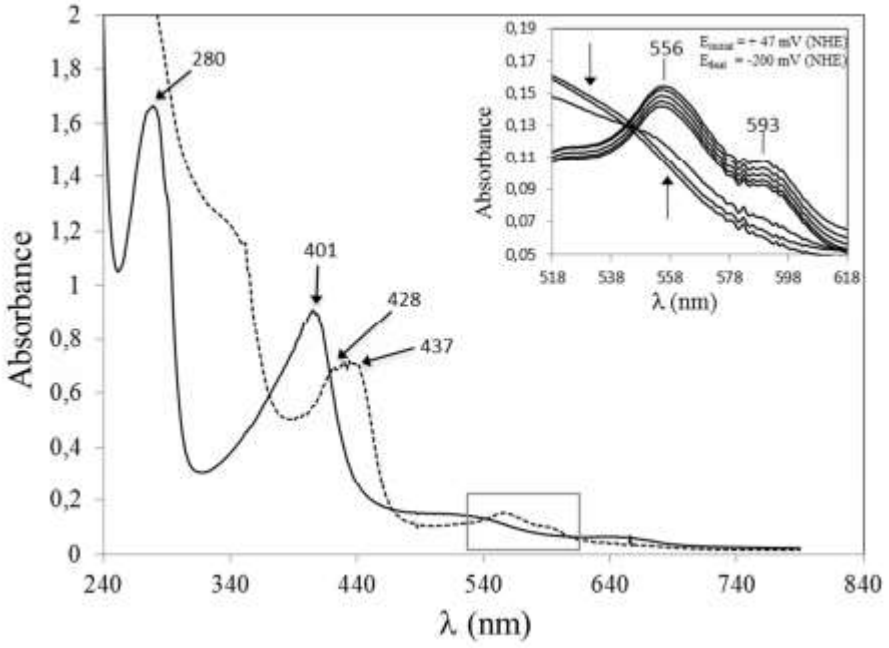

Fig. A5 X-band EPR for methaemoglobin. a) HSFe $^{3+}$ with g= 6 and b) LSFe^{3+} with g= 2.855, 2.226 and 1.794.[49]

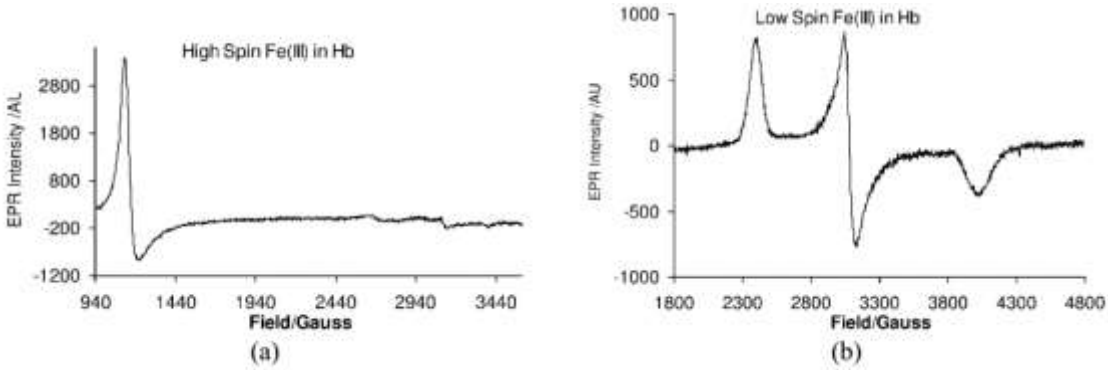

Fig. A6 Spectrochemical series.

Spectrochemical series:

$I^- < Br^- < SCN^- < Cl^- < F^- < OH^- < C_2O_4^{-2} < H_2O < NCS^- < NH_3 < en < bipy < CN^- < CO$

Δo_{SMALL} Δo_{LARGE}

Spectrochemical series in Biochemistry:

Asp/Glu < Cys < Tyr < Met < His < Lys < His^-

Δo_{SMALL} Δo_{LARGE}

Fig. A7 UV-Vis spectra showing the formation of Compound I (red line) during the reaction of BpKatG with PAA.[37]

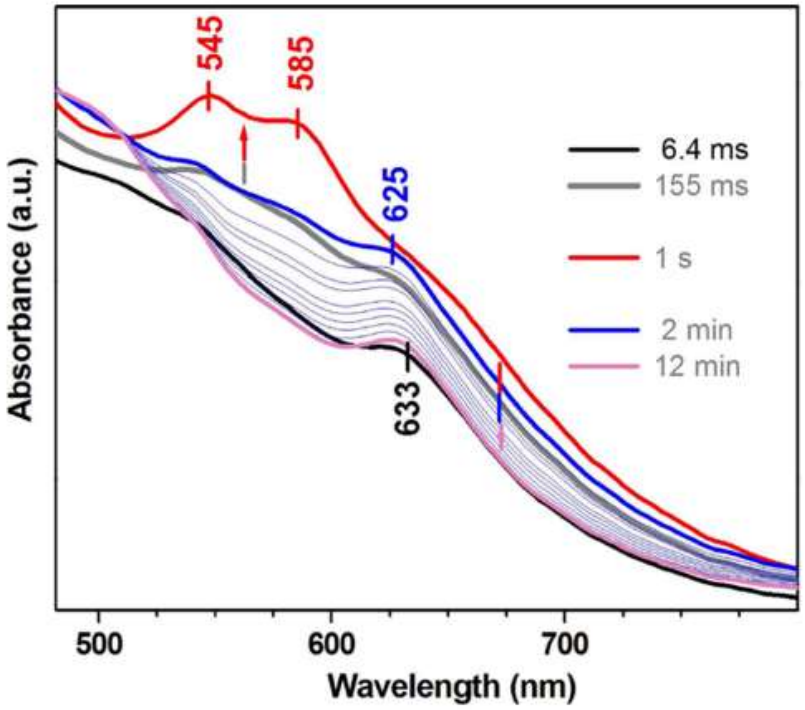

Fig. A8 X-band EPR spectrum at 100 K of the Fe^{2+}-Pheo complex synthesized from pheophytin and $FeCl_2$.